

Manifold learning: what, how, and why

Marina Meila,¹ Hanyu Zhang,²

November 8, 2023

Abstract

Manifold learning (ML), known also as non-linear dimension reduction, is a set of methods to find the low dimensional structure of data. Dimension reduction for large, high dimensional data is not merely a way to reduce the data; the new representations and descriptors obtained by ML reveal the geometric shape of high dimensional point clouds, and allow one to visualize, denoise and interpret them. This survey presents the principles underlying ML, the representative methods, as well as their statistical foundations from a practicing statistician’s perspective. It describes the trade-offs, and what theory tells us about the parameter and algorithmic choices we make in order to obtain reliable conclusions.

Contents

1	Introduction	2
2	Mathematical background	3
2.1	Notations	3
2.2	Manifold and Embedding	3
2.3	(Riemannian) geometry on manifolds and isometric embedding	4
3	Premises and paradigms in manifold learning	6
3.1	Neighborhood graphs	7
3.2	Linear local approximation	8
3.3	Principal curves and principal d -manifolds	8
4	Embedding algorithms	9
4.1	Review: Principal Component Analysis (PCA)	9
4.2	“One shot” embedding algorithms	10
4.2.1	Isomap	10
4.2.2	Diffusion Maps/Laplacian Eigenmaps	11
4.2.3	Local Tangent Space Alignment (LTSA)	12
4.3	“Horseshoe” effects, neighbor embedding algorithms, and selecting independent eigenvectors	13
4.3.1	Relaxation-based neighbor embedding algorithms	13
4.3.2	Avoiding the REP in spectral embeddings	14
4.4	Summary of embedding algorithms	16

5	Statistical basis of manifold learning	16
5.1	Biases in ML. Effects of sampling density and graph construction	18
5.2	Choosing the scale of neighborhood	18
5.3	Estimating the intrinsic dimension	20
5.4	Estimating the Laplace-Beltrami operator	21
5.5	Embedding distortions. Is isometric embedding possible?	22
6	Applications of manifold learning	24
6.1	Manifold learning in statistics	24
6.2	Manifold learning for visualization	25
6.3	Manifold learning in the sciences	25
7	Conclusion	26

1 Introduction

Modern data analysis tasks often face challenges of high dimension and thus nonlinear dimension reduction techniques emerge as a way to construct maps from high dimensional data to their corresponding low dimensional representations. Finding such low dimensional representations of high dimensional data is beneficial in several aspects. This saves space and processing time. More importantly, the low dimensional representation often provides a better understanding of the *intrinsic* structure of data, which often leads to better features that can be fed into further data analysis algorithms. This survey paper reviews the mathematical background, methodology, and recent development of nonlinear dimension reduction techniques. These techniques have been developed for two decades since two seminal works: Tenenbaum et al. (2000) and Roweis & Saul (2000), and are widely used in various data analysis jobs, especially in scientific research.

Before nonlinear dimension reduction emerged, Principal Component Analysis (PCA) was already widely accepted (I.T.Jolliffe, 2002). Intuitively, PCA assumes that high dimensional data living in \mathbb{R}^D lie around a lower dimensional linear subspace of \mathbb{R}^D and seeks to find the best linear subspace such that data points projected onto this subspace have minimal reconstruction error. Nonlinear dimension reduction algorithms extend this idea by assuming data are supported on smooth nonlinear low dimensional geometric objects, i.e., manifolds embedded in \mathbb{R}^D , and find maps that send the samples into lower dimensional coordinates while preserving some intrinsic geometric information.

In this survey, we start with a brief introduction to the main differential geometric concepts underlying ML, elaborating on the geometric information that manifolds carry (Section 2). Then, in Section 3, we describe the paradigm of manifold learning, with three possible sub-paradigms, each producing a different representation of the data manifold. The rest of the paper focuses on one of these, namely on the so-called embedding algorithms. In Section 4, we survey representative manifold learning algorithms and their variants. We also discuss the parameter choices, as well as some pitfalls, which leads to the discussion in Section 5, where we present the statistical aspects and statistical results supporting these methods. This section also includes the estimation of crucial manifold descriptors from data: the Laplace-Beltrami operator, Riemannian metrics, tangent space, intrinsic dimensions. Section 6 discusses applications, connecting with related statistics problems, and Section 7 concludes the survey.

2 Mathematical background

2.1 Notations

In this survey, we use the notation \mathbb{R}^D to represent the D -dimensional Euclidean space. A manifold is denoted as \mathcal{M} . Lowercase Greek letters such as $\varphi, \phi, \psi, \rho, \dots$ represent functions mapping from \mathcal{M} to a subset of Euclidean space, while English letters like f, g, h, \dots denote functions between real spaces. The notation C^ℓ refers to the class of functions with continuous derivatives up to order ℓ , and C^∞ represents the class of indefinitely differentiable functions. The Kronecker delta is symbolized by δ_{ij} . Bold lowercase English letters, like \mathbf{v} and \mathbf{x} , are used to denote vectors in Euclidean space. A dataset containing n data points is represented as the set $\mathcal{D} = \{\mathbf{x}_i\}_{i=1}^n$. Bold uppercase letters, such as $\mathbf{A}, \mathbf{B}, \mathbf{C}$, denote matrices. By convention, we treat a single data point as a column vector and use the matrix $\mathbf{X} \in \mathbb{R}^{n \times D}$ to represent the data matrix of a dataset with n data points, each being a vector in D -dimensional Euclidean space, while $\mathbf{Y} \in \mathbb{R}^{n \times m}$ will represent the same data mapped into m dimension by a manifold learning algorithm. The notation $\|\mathbf{v}\|$ signifies the ℓ_2 norm of vector \mathbf{v} . Throughout this survey, we also assume that all functions are *smooth*, i.e., continuously differentiable as many times as necessary.

2.2 Manifold and Embedding

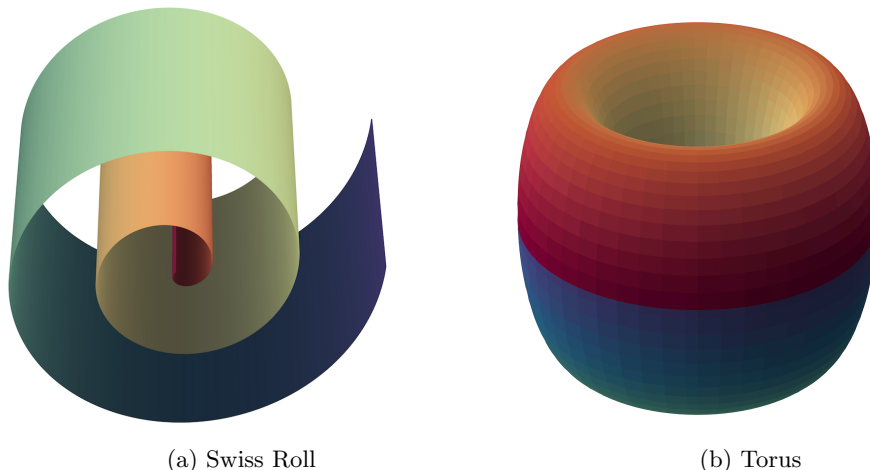
Manifolds and coordinate charts Readers are referred to Lee (2003), do Carmo (1992) for a rigorous introduction to manifolds and differential geometry. Intuitively, the notion of a manifold is a generalization of curves and surfaces. Mathematically, \mathcal{M} is a **smooth manifold** of dimension d (also called a d -manifold) if it is a topological space such that

- For each $\mathbf{p} \in \mathcal{M}$, there exists a mapping φ and an open neighborhood $U \subset \mathcal{M}$ of \mathbf{p} such that $\varphi : U \rightarrow \varphi(U)$ is bijective and both φ, φ^{-1} are smooth. Such pair (U, φ) is called a **chart**, and $\varphi^{-1} : \mathbb{R}^d \rightarrow \mathcal{M}$ is called **local coordinate**. Hence, local coordinates map tuples in \mathbb{R}^d to points on \mathcal{M} .
- For any two points $\mathbf{p}, \mathbf{p}' \in \mathcal{M}$ and two charts $(U, \varphi), (V, \phi)$ containing them, if $U \cap V \neq \emptyset$, then map $\varphi \circ \phi^{-1}$ is smooth on $\phi(U \cap V)$ and has a smooth inverse.

Hence, a smooth manifold is a set that locally around every point resembles an open set in Euclidean space and for which transitions between charts are seamless. Moreover, with the help of smooth coordinate charts, one can define differentiable functions of a manifold, or between two manifolds, in a natural way. Technically, \mathcal{M} is also required to be Hausdorff and second-countable. But most objects statisticians work with satisfy these conditions. Details about this mathematical definition of smooth manifolds can be found in the differential geometry textbook, such as do Carmo (1992).

The simplest example of a manifold is \mathbb{R}^d itself, which has a single, global coordinate chart. The “swiss roll” in Figure 1a is 2-manifolds that also admits a global coordinate chart (into \mathbb{R}^2). A sphere, or the torus in Figure 1b are also 2-manifolds, but they cannot be covered by a single chart (they each require at least two), as cartographers well know.

Note also that coordinate charts are not unique; $(U, \tilde{\phi})$ with $\tilde{\phi} = \tau \circ \phi$ is also a coordinate chart whenever $\tau : \phi(U) \rightarrow \mathbb{R}^d$ is smoothly invertible (τ in this case is a change of variables). While the multiplicity of charts, atlases and coordinate functions can be daunting at first sight, the framework of differential geometry is set up so that calculus, geometric, and topological quantities related to a manifold \mathcal{M} are independent of the coordinates chosen. For example, by compatibility, it follows that the dimension d must be the same for all charts and atlases. Hence, d is called the *intrinsic dimension* of the manifold \mathcal{M} .



For a data scientist, the above means that, (1), they can work in the coordinate system of their choice, and intrinsic quantities like d will remain invariant. But, (2), care must be taken when the low dimensional data from two different algorithms, or from different samples are being compared, because these may not be in the same coordinate system.

Embeddings In differential geometry, an *embedding* is a smooth map between two manifolds $F : \mathcal{M} \rightarrow \mathcal{N}$ whose inverse $F^{-1} : \mathcal{F}(\mathcal{M}) \subset \mathcal{N} \rightarrow \mathcal{M}$ exists and is also smooth. Of special interest is the case $\mathcal{M} \subset \mathcal{N}$; then \mathcal{M} is said to be a submanifold of \mathcal{N} . Commonly in statistics, the high dimensional data lie originally in $\mathcal{N} = \mathbb{R}^D$, and we model them by \mathcal{M} a submanifold of \mathbb{R}^D to be estimated. Then D is called the ambient dimension (of the data). The ML algorithms that we will focus on can be seen as finding an embedding $F : \mathcal{M} \rightarrow \mathbb{R}^m$, with $m \geq d$ and $m \ll D$; in particular, if $m = d$, the embedding F is a (global) coordinate chart.

An advantage of embeddings is that one can avoid using multiple charts to describe a manifold. Instead, one can find a global mapping $F : \mathcal{M} \subset \mathbb{R}^D \rightarrow \mathcal{N} \subset \mathbb{R}^m$, where \mathcal{N} is easier to understand. Whitney’s embedding Theorem (Lee, 2003) states that every d -dimensional manifold can be embedded into \mathbb{R}^{2d} . Therefore, if one can find a valid embedding, a significant dimension reduction can be achieved (from D to $O(d)$). This is one of the major targets of manifold learning algorithms.

This section has introduced manifolds as spaces that are “like \mathbb{R}^d ” locally around a point \mathbf{p} . Next, we show how concepts such as distances and angles, that is, Euclidean geometry, are transferred from \mathbb{R}^d to d -manifolds.

2.3 (Riemannian) geometry on manifolds and isometric embedding

For the data in Figure 2, a scientist may be interested in the distance between two molecular configurations $\mathbf{x}_1, \mathbf{x}_2$, seen as points of $\mathcal{M} \subset \mathbb{R}^D$. Their Euclidean distance $\|\mathbf{x}_1 - \mathbf{x}_2\|$ is readily available without requiring any additional statistics. However, this value may not be of physical interest, since most of the putative configurations along the segment \mathbf{x}_1 to \mathbf{x}_2 in \mathbb{R}^D are not physically possible. To deform from state \mathbf{x}_1 to \mathbf{x}_2 , the ethanol molecule must follow a path contained in (or near) the manifold \mathcal{M} of possible configurations, and the distance $d_{\mathcal{M}}(\mathbf{x}_1, \mathbf{x}_2)$ shall naturally be defined as the shortest possible length of such a path (and is called the *geodesic distance*). Just like in \mathbb{R}^d the distance between two points is independent of the choice of

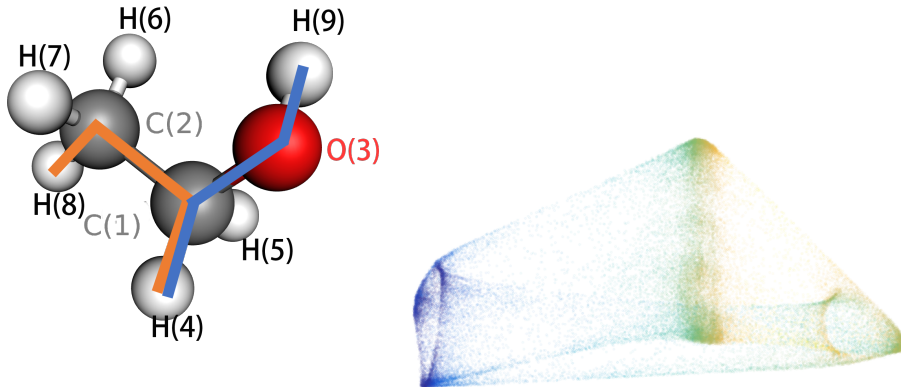


Figure 2: **Left:** The ethanol molecule has 9 atoms; a spatial configuration of ethanol has $D = 3 \times 9$ dimensions. The CH_3 group (atoms 2,6,7,8) and the OH group (atoms 3,9) can rotate w.r.t. the middle group (atoms 1,4,5), and the blue and orange lines represent these angles of rotation. **Right:** A 2-manifold estimated from 50,000 configurations of the ethanol molecule. The manifold has the topology of a torus, and the color represents the rotation of the OH group. The sharp “corners” are distortions introduced by the embedding algorithm (explained in Section 5.1). Figure 6 shows the original data. This dataset is from Chmiela et al. (2017)

basis, and invariant if \mathbb{R}^d is a subspace of a larger Euclidean space, distances along curves in a manifold \mathcal{M} can be defined solely based on the coordinate charts (U, ϕ) , hence *intrinsically*, without reference to the ambient space \mathbb{R}^D , and are purely geometric, hence are independent of the choices of charts. This is achieved through Riemannian geometry, as follows.

In \mathbb{R}^d , the scalar product $\langle \mathbf{v}, \mathbf{u} \rangle = \mathbf{v}^T \mathbf{u}$ is sufficient to define both distances, by $\|\mathbf{v} - \mathbf{u}\|^2 = \langle \mathbf{v} - \mathbf{u}, \mathbf{v} - \mathbf{u} \rangle$, and angles, by $\angle(\mathbf{v}, \mathbf{u}) = \cos^{-1}(\langle \mathbf{v}, \mathbf{u} \rangle / (\|\mathbf{v}\| \|\mathbf{u}\|))$. Moreover, any positive definite matrix $\mathbf{A} \in \mathbb{R}^{d \times d}$ can induce an inner product by $\langle \mathbf{v}, \mathbf{u} \rangle_{\mathbf{A}} = \mathbf{v}^T \mathbf{A} \mathbf{u}$; in this context, \mathbf{A} is often called a *metric* on \mathbb{R}^d .

Riemann took up this idea and introduced the *Riemannian metric*, which plays the same role as \mathbf{A} above; however, this metric is allowed to vary from point to point, smoothly.

Tangent space and Riemannian metric The *tangent space* $\mathcal{T}_{\mathbf{p}}\mathcal{M}$ at a point $\mathbf{p} \in \mathcal{M}$ is a d -dimensional vector space of *tangent vectors* to \mathcal{M} . The canonical basis of $\mathcal{T}_{\mathbf{p}}\mathcal{M}$ is given by the tangents to the coordinate functions seen as curves on \mathcal{M} , while the tangent vectors can be seen as tangents (or velocity vectors) at \mathbf{p} to smooth curves on \mathcal{M} passing through \mathbf{p} . The collection of tangent spaces $\mathcal{T}_{\mathbf{p}}\mathcal{M}$ for all points $\mathbf{p} \in \mathcal{M}$, is called the tangent bundle of \mathcal{M} , denoted by \mathcal{TM} .

A *Riemannian metric* \mathbf{g} of a manifold \mathcal{M} associates to each point $\mathbf{p} \in \mathcal{M}$ an inner product $\langle \cdot, \cdot \rangle_{\mathbf{g}(\mathbf{p})}$ on the tangent space $\mathcal{T}_{\mathbf{p}}\mathcal{M}$, which varies smoothly on \mathcal{M} . The inner product \mathbf{g} defines on each tangent space the norm $\|\mathbf{v}\|_{\mathbf{g}} = \sqrt{\langle \mathbf{v}, \mathbf{v} \rangle_{\mathbf{g}}}$, distance $\|\mathbf{v}_1 - \mathbf{v}_2\|_{\mathbf{g}}$, angle $\cos^{-1}(\langle \mathbf{v}_1, \mathbf{v}_2 \rangle_{\mathbf{g}} / (\|\mathbf{v}_1\|_{\mathbf{g}} \|\mathbf{v}_2\|_{\mathbf{g}}))$ for all vectors in $\mathcal{T}_{\mathbf{p}}\mathcal{M}$. More importantly, infinitesimal quantities such as the line element $dl = \sum_{i,j=1}^d \mathbf{g}_{ij} dx^i dx^j$ and volume element $dV = \sqrt{\det(\mathbf{g})} dx^1 \cdots dx^d$ are also expressed through the Riemannian metric, allowing one to define lengths of curves and volumes of subsets of \mathcal{M} as integrals. These integrals are invariant to the choice of bases in \mathcal{TM} , hence to the choice of

Table 1: Three main paradigms for non-linear dimension reduction

Paradigm	Representation	
Linear local	$\mathbf{x}_i \in U \subset \mathcal{M} \xrightarrow{F} \mathbf{v}_i \in \hat{\mathcal{T}}_{\mathbf{p}}\mathcal{M} \cong \mathbb{R}^d$	$D \rightarrow d$, local coordinates only
Principal Curves and Surfaces	$\mathbf{x}_i \in \mathbb{R}^D \xrightarrow{F} \mathbf{x}'_i \in \mathcal{M} \subset \mathbb{R}^D$	$D \rightarrow D$, global coordinates, noise removal
Embedding	$\mathbf{x}_i \in \mathcal{M} \xrightarrow{F} \mathbf{y}_i \in F(\mathcal{M}) \subset \mathbb{R}^m$	$D \rightarrow m$, with $m \geq d$, global coordinates (or charts)

coordinate charts on \mathcal{M} .

Isometry and isometric embedding A smooth map $F : \mathcal{M} \rightarrow \mathcal{N}$ induces linear maps $dF_{\mathbf{p}} : \mathcal{T}_{\mathbf{p}}\mathcal{M} \rightarrow \mathcal{T}_{F(\mathbf{p})}\mathcal{N}$ called the *differential* of F at \mathbf{p} . If we fix the coordinate systems on \mathcal{M} and \mathcal{N} , $dF_{\mathbf{p}}$ becomes a $\dim \mathcal{N} \times \dim \mathcal{M}$ matrix which maps $\mathbf{v} \in \mathcal{T}_{\mathbf{p}}\mathcal{M}$ to $dF_{\mathbf{p}}\mathbf{v} \in \mathcal{T}_{F(\mathbf{p})}\mathcal{N}$ (i.e., the *Jacobian* of F in the given coordinates).

A smooth map $F : \mathcal{M} \rightarrow \mathcal{N}$ between Riemannian manifolds $(\mathcal{M}, \mathbf{g}), (\mathcal{N}, \mathbf{h})$, is an *isometry* if the Riemannian metric \mathbf{g} at each point \mathbf{p} is preserved by F , i.e. iff

$$\text{for all } \mathbf{p} \in \mathcal{M} \text{ and } \mathbf{v}_1, \mathbf{v}_2 \in \mathcal{T}_{\mathbf{p}}\mathcal{M}, \quad \langle \mathbf{v}_1, \mathbf{v}_2 \rangle_{\mathbf{g}(\mathbf{p})} = \langle dF_{\mathbf{p}}(\mathbf{v}_1), dF_{\mathbf{p}}(\mathbf{v}_2) \rangle_{\mathbf{h}(F(\mathbf{p}))} \quad (1)$$

An isometry F preserves geometry quantities such as angles, distances, path lengths, volumes etc. An embedding that is also an isometry is called an *isometric embedding*.

Ideally, we would like a manifold learning algorithm to produce an embedding F into \mathbb{R}^m that is isometric. Here we face one of the most remarkable gaps between mathematical theory and methodology in manifold learning. Although it was long proved (Nash embedding theorem (Lee, 2003)) that isometric embedding is possible, no known practical algorithm capable of isometric embedding exists at this time (details and refinement of this statement are in Section 5.5). However, by estimating auxiliary information, working with a non-isometric embedding as if it was isometric is still possible (see Section 5.5).

3 Premises and paradigms in manifold learning

The Manifold Assumption Suppose we are given data $\{\mathbf{x}_i\}_{i=1}^n$ where each data entry $\mathbf{x}_i \in \mathbb{R}^D$. It is assumed that data are sampled from a distribution \mathbb{P} that is supported on, or close to a d dimensional manifold \mathcal{M} embedded in \mathbb{R}^D . This is the *Manifold Assumption*. Throughout this survey, with a few noted exceptions, we will discuss the no noise case, when the data lie exactly on \mathcal{M} .

Manifold learning A manifold learning algorithm can be thought as a mapping F of $\mathbf{x}_i \in \mathbb{R}^D$ to $\mathbf{y}_i \in \mathbb{R}^m$. The *embedding dimension* m is usually much smaller than D but could be higher than the intrinsic dimension d . In the regime that \mathbb{P} is supported exactly on \mathcal{M} , and sample size $n \rightarrow \infty$, a valid manifold learning algorithm F should converge to a smooth embedding function F . This implies that the algorithm should be guaranteed to recover the manifold \mathcal{M} , regardless of the shape of \mathcal{M} .

Once the manifold assumption is believed to be true, most manifold learning and non-linear dimension reduction methods can be grouped into three paradigms, which differ in the way they represent the recovered manifold. They are local linear approximations (Section 3.2), Principal Curves and Surfaces (3.3), and embedding algorithms, which will be the focus of Section 4.

The Manifold Assumption itself is testable. For example in Fefferman et al. (2016), tests whether, given an i.i.d. sample, there exists a manifold \mathcal{M} that can approximate this sample with tolerance ε . These results are currently not practically useful, as knowledge of usually unknown parameters of the manifold (d , reach, volume) must be known or estimated. However, they, as well as Genovese et al. (2012), give us the confidence to develop and use ML algorithms in practice.

3.1 Neighborhood graphs

Practically all manifold learning algorithms start with finding the neighbors of each data point \mathbf{x}_i . This leads to the construction of a *neighborhood graph*; this graph, with suitable weights, summarizing the local geometric and topological information in the data, is the typical input to a non-linear dimension reduction algorithm. Every data point \mathbf{x}_i represents a node in this graph, and two nodes are connected by an edge if their corresponding data points are neighbors. Throughout the survey, we use \mathcal{N}_i to denote the neighbors of \mathbf{x}_i and $k_i = |\mathcal{N}_i|$ be the number of neighbors of \mathbf{x}_i (including \mathbf{x}_i itself). The matrix $\mathbf{N}_i \in \mathbb{R}^{k_i \times D}$ is the matrix with each row representing a neighbor of \mathbf{x}_i .

There are two usual ways to define neighbors. In a *radius-neighbor graph*, \mathbf{x}_j is a neighbor of \mathbf{x}_i iff $\|\mathbf{x}_i - \mathbf{x}_j\| \leq r$. Here r is a parameter that controls the neighborhood scale, similar to a bandwidth parameter in kernel density estimation. Consistency of manifold learning algorithms is usually established assuming an appropriately selected neighborhood size, that decreases slowly with n (see Section 5.2). In the *k-nearest neighbor (k-NN) graph*, \mathbf{x}_j is the neighbor of \mathbf{x}_i iff \mathbf{x}_j is among the closest k points to \mathbf{x}_i . Since this relation is not symmetric, usually the neighborhoods are symmetrized to obtain an undirected neighborhood graph.

The k -NN graph has many computational advantages w.r.t. the radius neighbor graph; it is more regular and often it is connected when the latter is not. More software is available to construct (approximate) k -NN graphs fast for large data. But theoretically, it is much more difficult to analyze, and fewer consistency results are known for k -NN graphs (Sections 5.1, 5.4). Intuitively, k_i the number of neighbors in the radius graph is proportional to the local data density, and manifold estimation can be analyzed through the prism of kernel regression; while the k -NN graph is either asymmetric, or if symmetrized, becomes more complicated to analyze.

The distances between neighbors are stored in the distance matrix \mathbf{A} , with \mathbf{A}_{ij} being the distance $\|\mathbf{x}_i - \mathbf{x}_j\|$ if $\mathbf{x}_j \in \mathcal{N}_i$, and infinity if \mathbf{x}_j is not a neighbor of \mathbf{x}_i .

Some algorithms weight the neighborhood graph by weights that are non-increasing with distances; the resulting $n \times n$ matrix is called the *similarity matrix* (or sometimes *kernel matrix*). The weights are given by a *kernel function*,

$$\mathbf{K}_{ij} := \begin{cases} K\left(\frac{\|\mathbf{x}_i - \mathbf{x}_j\|}{h}\right), & \mathbf{x}_j \in \mathcal{N}_i, \\ 0, & \text{otherwise.} \end{cases} \quad (2)$$

The kernel function here is almost universally the Gaussian kernel, defined as $K(u) = \exp(-u^2)$ (Belkin et al. (2006), Ting et al. (2010), Coifman & Lafon (2006), Singer & Wu (2012), etc). In the above, h , the kernel width, is another hyperparameter that must be tuned. Note that, even if \mathcal{N}_i would trivially contain all the data, the similarity \mathbf{K}_{ij} vanishes for far-away data points. Therefore, equation (2) effectively defines a radius-neighbor graph with $r \propto h$. Hence, a rule of thumb is to select r to be a small multiple of h (e.g., 3–10 h).

It is sometimes also useful to have kernel function $K(u) = \mathbf{1}$. Then the similarity matrix \mathbf{K} is the same as the unweighted adjacency matrix of the radius neighbor graph. By construction, \mathbf{K} is usually a sparse matrix, which is useful to accelerate the computation.

If the data is so that D is large, which is often the case, and n is large too, which is necessary for manifold recovery, constructing the neighborhood graph can be the most computationally demanding step of the algorithm. Fortunately, much work has been devoted to speeding up this task, and approximate algorithms are now available, which can run in almost linear time in n (computation complexity can be reduced to $O(n^{1+\delta})$, where $\delta < 1$ is a positive constant) and have very good accuracy (Ram et al. (2009)).

Next, we briefly describe two of the paradigms in Table 1, then, from Section 4 on focus on the third, embedding algorithms.

3.2 Linear local approximation

This idea stems from the classical Principal Component Analysis, and it seeks to adapt it to data sampled from a curved manifold, instead of a linear subspace. Random projections (Baraniuk & Wakin, 2009, Hegde et al., 2007) were first proposed to learn the structure of a low dimensional manifold. Let $F : \mathbb{R}^D \rightarrow \mathbb{R}^m$ be a random orthogonal projector¹, it is sufficient to have $m \geq O(d \log n / \varepsilon^2)$ to preserve all distances approximately, in the sense that $(1 - \varepsilon)\sqrt{m/n} \leq \text{dist}(F(\mathbf{x}_i), F(\mathbf{x}_j)) / \text{dist}(\mathbf{x}_i, \mathbf{x}_j) \leq (1 + \varepsilon)\sqrt{m/n}$ holds for any $\mathbf{x}_i, \mathbf{x}_j$ from \mathcal{M} . Here dist can be either geodesic distance on \mathcal{M} or Euclidean distance on \mathbb{R}^D . For large data, however, this approach leads to a large m , not useful for dimension reduction.

Both PCA and random projections seek global linear representations, and they do not utilize the geometric structure of the manifold in a finer scale at a reference point \mathbf{x} . One improvement is to perform PCA on a weighted covariance matrix, with weights decaying away from \mathbf{x} , i.e. let

$$\mathbf{C} = \frac{1}{n} \sum_{i=1}^n w_i (\mathbf{x}_i - \mathbf{x})(\mathbf{x}_i - \mathbf{x})^\top. \quad (3)$$

The weights can be computed using the kernel $K(\cdot)$ and bandwidth h used for the neighborhood graph, for example. This weighted PCA procedure is sometimes termed *local PCA (lPCA)*. Local PCA is only used to understand geometric structure near any reference point, usually one of the points in \mathcal{D} . One can map all the data by performing lPCA with a subset of the data points so that each \mathbf{x}_i is sufficiently well approximated by its projection. This way, all the data are represented in d dimensional coordinates. However, some points can have more than one representation, if they are close to 2 or more reference points. All the representations (i.e., coordinates) are *local*, and understanding or making inferences on the entire manifold are tedious at best. This approach can be refined into a multiscale local linear approach, which is more accurate and parsimonious (Chen et al., 2013).

3.3 Principal curves and principal d -manifolds

This paradigm is the only one of the three where noise is assumed. Consider data of the form $\mathbf{x}_i = \mathbf{x}_i^* + \epsilon_i$, where ϵ_i represents 0-mean noise, and the \mathbf{x}_i^* are sampled from a curve, for instance. Then, to recover the curve, one would need to estimate the local mean of the data, and this was proposed in the seminal work of Hastie & Stuetzle (1989); unfortunately, the estimation is difficult, and this definition does not lead to a unique curve. A more recent proposal that removed the previous difficulties was to define the principal curve as the *ridge* of the data density. point \mathbf{x} is on a ridge if it is a local maximum of the density $f_{\mathbf{x}}$ in $D - 1$ directions, and the remaining direction coincides with the gradient $\nabla f_{\mathbf{x}}$. Several ridges may meet at a peak, i.e., at a local

¹Obtained by orthogonalizing a matrix with i.i.d. normal or Bernoulli entries

maximum, but in between, the ridges are manifolds (Chen et al., 2015) if the density $f_{\mathbf{x}}$ is smooth enough. This concept can be extended to principal surfaces, and principal d -manifolds.

The ridge can be estimated with the *Subspace Constrained Mean Shift (SCMS)* algorithm (for more details, we refer the reader to Ozertem & Erdogmus (2011)). The SCMS algorithm maps each \mathbf{x}_i to a point $\mathbf{y}_i \in \mathbb{R}^D$ lying on the principal curve (or d -manifold). Hence, as a manifold estimation algorithm, this method does not reduce dimension. However, unlike local linear maps, the output is in a global coordinate system, i.e. \mathbb{R}^D .

Usually, the ridge does not coincide with the mean of the data; the bias depends on the curvature of the manifold: the density is higher on the “inside” of the curve. However, for their smoothing property, principal d -manifolds are remarkably useful in the analysis of manifold estimation in noise (Genovese et al., 2012, Mohammed & Narayanan, 2017).

We have quickly reviewed two simple methods for manifold estimation: local linear approximation reduces the dimension locally, but offers no global representation, while principal curves produce a global representation but do not reduce dimension. It is time to focus on the third class, of algorithms that produce embeddings, representations that are both global and low dimension.

4 Embedding algorithms

The term “manifold learning” was proposed in the seminal work of two algorithms: LLE (Roweis & Saul (2000)) and ISOMAP (Tenenbaum et al. (2000)), together inaugurated the modern era of non-linear dimension reduction. In this subsection, we introduce classical manifold learning algorithms that (attempt to) find a global embedding $\mathbf{Y} \in \mathbb{R}^{n \times m}$ of data set \mathcal{D} .

We separate the algorithms, roughly, into “one-shot” algorithms, which obtain embedding coordinates from the principal eigenvectors of some matrix derived from the neighborhood graph, or by solving some other global (usually convex) optimization problem, and “attraction-repulsion” algorithms, which proceed from an initial embedding \mathbf{Y} (often produced by a one-shot algorithm) and improve it iteratively. While this taxonomy can rightly be called superficial, at present, it represents a succinct and relatively accurate summary of the state of the art.

No matter what the approach, given the neighborhood information summarized in the weighted neighborhood graph, an embedding algorithm’s task is to produce a smooth mapping of the inputs which distorts the neighborhood information as little as possible. The algorithms that follow differ in their choice of information to preserve, and in the sometimes implicit constraints on smoothness.

4.1 Review: Principal Component Analysis (PCA)

Before we dive deep into various non-linear dimension reduction algorithms, we have a brief review on linear dimension reduction methods.

Linear dimension reduction methods find global embedding of the data in a low dimensional linear subspace. One way of understanding principal component analysis is to find d dimensional linear subspace \mathcal{V} such that the data $\{\mathbf{x}_i\}$ projected onto it have the smallest reconstruction error. If \mathcal{V} has an orthogonal basis $\mathbf{T} \in \mathbb{R}^{D \times d}$ such that $\mathbf{T}^\top \mathbf{T} = \mathbf{I}_d$. Then \mathbf{x}_i projected onto \mathcal{U} has low dimensional representation $\mathbf{y}_i = \mathbf{T}^\top \mathbf{x}_i$ under basis \mathbf{T} . In \mathbb{R}^D , projection of \mathbf{x}_i onto \mathcal{U} is given by $\mathbf{T}\mathbf{T}^\top \mathbf{x}_i$. If we introduce the data matrix $\mathbf{X} \in \mathbb{R}^{n \times D}$, with i -th row being \mathbf{x}_i^\top , then the low dimensional representation matrix $\mathbf{Y} \in \mathbb{R}^{n \times d}$ is given by $\mathbf{X}\mathbf{T}$ and in \mathbb{R}^D the projected data matrix is $\mathbf{X}\mathbf{T}\mathbf{T}^\top$.

Then we can write PCA problem as

$$\min_{\mathbf{T}: \mathbf{T} \in \mathbb{R}^{D \times d}, \mathbf{T}^\top \mathbf{T} = \mathbf{I}_d} \sum_{i=1}^n \|\mathbf{x}_i - \mathbf{T} \mathbf{T}^\top \mathbf{x}_i\|^2 = \min_{\mathbf{T}: \mathbf{T} \in \mathbb{R}^{D \times d}, \mathbf{T}^\top \mathbf{T} = \mathbf{I}_d} \|\mathbf{X} - \mathbf{X} \mathbf{T} \mathbf{T}^\top\|_F^2 \quad (4)$$

Consider the singular value decomposition preserving only the first d singular values of $\mathbf{X} = \mathbf{U} \mathbf{\Sigma} \mathbf{V}^\top$ where $\mathbf{U} \in \mathbb{R}^{n \times d}$, $\mathbf{V} \in \mathbb{R}^{D \times d}$ are orthogonal matrices and $\mathbf{\Sigma}$ is $d \times d$ diagonal matrix, then solution of this problem is $\mathbf{T} = \mathbf{V}$. Low dimensional representation of original data is $\mathbf{Y} = \mathbf{X} \mathbf{T} = \mathbf{U} \mathbf{\Sigma}$, these are also called principal components. In the terminology of PCA, columns of \mathbf{V} are called principal vectors. They characterize the directions that explain the variance in the data.

When data \mathbf{x}_i are centered, the (unnormalized) sample covariance matrix of data is $\mathbf{C} = \mathbf{X}^\top \mathbf{X}$. The solution to PCA can also be found by eigendecomposition of \mathbf{C} . The first d eigenvectors of \mathbf{C} is just matrix \mathbf{V} . If the dimension $D \gg n$, it will be easier to first compute the Gram matrix $\mathbf{C} = \mathbf{X}^\top \mathbf{X}$ and then perform a truncated eigen-decomposition $\mathbf{C} = \mathbf{V} \mathbf{\Sigma}^2 \mathbf{V}^\top$. Low dimensional representation is still $\mathbf{X} \mathbf{V}$.

4.2 “One shot” embedding algorithms

4.2.1 Isomap

Classical Multidimensional Scaling (MDS, Kruskal (1964)) takes input from a pairwise distance matrix \mathbf{A} and outputs coordinates $\mathbf{Y} \in \mathbb{R}^d$ that best preserve the distances. ISOMAP is a generalization of multidimensional scaling that preserves distances between data points while finding low dimensional coordinates. Instead of Euclidean distance in classical MDS, ISOMAP use shortest path distances in the neighborhood distance graph to approximate geodesic distance on a manifold.

Algorithm 1 ISOMAP

Input: : Neighborhood distance matrix \mathbf{A} , embedding dimension m

1: Compute shortest path distance matrix $\tilde{\mathbf{A}}_{ij}$:

$$\tilde{\mathbf{A}}_{ij} = \begin{cases} \mathbf{A}_{ij} & \mathbf{A}_{ij} < \infty, \\ \text{shortest path distance between } i, j & \mathbf{A}_{ij} = \infty. \end{cases}$$

2: Multidimensional Scaling $\mathbf{Y} = \text{MDS}(\mathbf{M}, d)$ with $hM = [\tilde{\mathbf{A}}_{ij}^2]$

Output: : m dimensional coordinates \mathbf{Y} for \mathcal{D}

Intuitively, the shortest graph distance is a good approximation to the geodesic distance in a neighborhood provided that data are sufficiently dense in this region and neighborhood size is appropriately chosen (Bernstein et al., 2000). In the limit of large n , ISOMAP was shown to produce isometric embeddings for $m = d$, whenever the data manifold is *flat*, i.e. admits an isometric embedding in \mathbb{R}^d , and data space is convex. Empirically, ISOMAP embeddings are close to isometric also when $m > d$ and m is sufficient for isometric embedding.

Computation complexity of ISOMAP is $O(n^3)$, with a most computational burden for computing all pairs of shortest path distance. Space complexity is $O(n^2)$. Since ISOMAP works with dense matrices, this space complexity cannot be improved.

There are variants of Isomap that improve it in different ways: Hessian Eigenmap (Donoho & Grimes, 2003) enables non-convex data where they introduce the use of Hessian operator;

Continuum Isomap (Zha & Zhang, 2007) generalizes Isomap to a continuous version such that out-of-sample extension of Isomap is possible.

4.2.2 Diffusion Maps/Laplacian Eigenmaps

Unlike ISOMAP, DM, as well as most embedding methods, work with a sparse matrix derived from the similarity \mathbf{K} ; namely, they embed the data by the eigenvectors of the *graph Laplacian* \mathbf{L} . The construction of \mathbf{L} , also called the *Diffusion Maps Laplacian* or *renormalized Laplacian*, is described in Algorithm 3 (and it consists of a column normalization of \mathbf{K} , followed by a row normalization). The LE algorithm differs from DM only in the use of a different Laplacian, \mathbf{L}^{norm} below.

Algorithm 2 DIFFUSION MAPS/LAPLACIAN EIGENMAPS

Input: Graph Laplacian \mathbf{L} (or \mathbf{L}^{nor} , embedding dimension m).

- 1: Compute eigenvectors of smallest $m + 1$ eigenvalues of \mathbf{L} , $\{\mathbf{v}^i\}_{i=0}^m$, each eigenvector $\mathbf{v}^i \in \mathbb{R}^n$.
- 2: Discard \mathbf{v}^0 .
- 3: Represent each \mathbf{x}_j by $\mathbf{y}_j = (v_j^1, \dots, v_j^m)^\top$

Output: \mathbf{Y}

To construct a graph Laplacian matrix, let $d_i = \sum_{j \in \mathcal{N}_i} \mathbf{K}_{ij}$ represent the degree of node i and $\mathbf{D} = \text{diag}\{d_1, \dots, d_n\}$. Then multiple choices of graph Laplacian exist:

- Unnormalized Laplacian: $\mathbf{L}^{un} = \mathbf{D} - \mathbf{K}$
- Normalized Laplacian: $\mathbf{L}^{nor} = \mathbf{I} - \mathbf{D}^{-1/2} \mathbf{K} \mathbf{D}^{-1/2}$
- Random-walk Laplacian: $\mathbf{L}^{rw} = \mathbf{I} - \mathbf{D}^{-1} \mathbf{K}$
- Renormalized Laplacian \mathbf{L} described below.

Algorithm 3 Renormalized Laplacian

Input: Neighborhood similarity matrix \mathbf{K} , kernel function $k()$ and kernel bandwidth h

Compute similarity matrix $\mathbf{K}_{ij} = k(\mathbf{A}_{ij}/h)$

Normalize columns: $d_j = \sum_{i=1}^n \mathbf{K}_{ij}$, $\tilde{\mathbf{K}}_{ij} = \mathbf{K}_{ij}/d_j$ for all $i, j = 1, \dots, n$

Normalize rows: $d'_i = \sum_{j=1}^n \tilde{\mathbf{K}}_{ij}$, $\mathbf{P}_{ij} = \tilde{\mathbf{K}}_{ij}/d'_i$ for all $i, j = 1, \dots, n$

Output: $\mathbf{L} = (\mathbf{I} - \mathbf{P})/h^2$

Why one Laplacian rather than another? The reason is that, even though in many simple examples the difference is hard to spot, one needs to ensure that, as more sample sizes are collected, the limit of these \mathbf{L} 's is well defined, and the embedding algorithm is unbiased. It is easy to see that \mathbf{L}^{norm} and \mathbf{L}^{rw} are similar matrices. Moreover, whenever the degrees d_i are constant, $\mathbf{L} = \mathbf{L}^{rw} \propto \mathbf{L}^{un}$, hence all Laplacians should produce the same embedding. The difference appears when the data density is non-uniform, making one \mathbf{x}_i be surrounded more densely by other data points. The seminal work Coifman & Lafon (2006), which introduced renormalization, showed that in this case, the eigenvectors of $\mathbf{L}^{norm}, \mathbf{L}^{rw}$ are biased by the sampling density and that renormalization removes this bias. Sections 5.4, and Figure 6 illustrate this.

The idea of *spectral embedding* appeared in (Shi & Malik, 2000, Belkin & Niyogi, 2002) as a trick for clustering, and was then generalized as a data representation method in Belkin & Niyogi (2003) as LE. They connect the graph Laplacian with the famous Laplace-Beltrami operator $\Delta_{\mathcal{M}}$ of manifold, a differential operator that plays an important role in modern differential geometry (Rosenberg, 1997). Estimating the Laplace-Beltrami operator itself is an important geometric estimation problem that will be reviewed in Section 5.4.

Because \mathbf{L} is sparse, DM/LE are computationally less challenging when compared with ISOMAP.

4.2.3 Local Tangent Space Alignment (LTSA)

This algorithm, proposed in (Zhang & Zha, 2004) seeks to find local representation in the tangent space at each point \mathbf{x}_i , then aligns these to obtain global coordinates.

The first stage of LTSA finds the local representation of neighboring points $j \in \mathcal{N}_i$ via projections on the tangent $\mathcal{T}_{\mathbf{x}_i}\mathcal{M}$; thus $\mathbf{y}_j - \mathbf{y}_i$ can locally be approximated by an affine transformation of orthogonal projections of \mathbf{x}_j onto tangent space at \mathbf{x}_i through Taylor expansion. The optimal affine transformation is obtained by minimizing the reconstruction error near each \mathbf{x}_i

$$\min_{\tilde{\mathbf{x}}_i, \Theta, \mathbf{Q}} \sum_{j \in \mathcal{N}_i} \|\mathbf{x}_j - (\tilde{\mathbf{x}}_i + \mathbf{Q}\theta_j^{(i)})\|^2, \quad (5)$$

Where \mathbf{x}, \mathbf{Q} are translation and rotation that parametrize this affine transformation. θ_j is a local coordinate of each neighbor \mathbf{x}_j projected on this linear subspace.

In the second stage of LTSA, one obtains global embedding coordinates \mathbf{Y} while θ_j that preserves local geometry information, through minimizing a global reconstruction error

$$\min_{\{\mathbf{y}_i\}_{i=1}^n, \{\mathbf{P}_i\}_{i=1}^n} \sum_{i=1}^n \sum_{j \in \mathcal{N}_i} \|\mathbf{y}_j - \tilde{\mathbf{y}}_i - \mathbf{P}_i\theta_j^{(i)}\|^2 \quad (6)$$

The optimization in both steps can be transformed into eigenvalue problems. Hence the algorithmic procedure of LTSA is displayed in algorithm 4

Algorithm 4 LOCAL TANGENT SPACE ALIGNMENT

Input: Dataset \mathcal{D} , embedding dimension m .

$\mathbf{B} = \mathbf{0}$

for $i = 1, 2, \dots, n$ **do**

Find the k nearest neighbors of \mathbf{x}_i : $\mathbf{x}_j, j \in \mathcal{N}_i$.

Find local dataset $\Xi_i = [\mathbf{x}_j - \tilde{\mathbf{x}}_i]_{j \in \mathcal{N}_i}$, where $\tilde{\mathbf{x}}_i$ is the average of all neighbors of \mathbf{x}_i .

Compute the m largest eigenvectors $\tilde{\mathbf{v}}^1, \dots, \tilde{\mathbf{v}}^d$ of $\Xi_i^\top \Xi_i$, set $\mathbf{G}_i = [1/\sqrt{k}, \tilde{\mathbf{v}}^1, \dots, \tilde{\mathbf{v}}^d]$

$\mathbf{B} = \mathbf{B} + \mathbf{I} - \mathbf{G}_i \mathbf{G}_i^\top$.

end for

Compute the 2 to $m + 1$ smallest eigenvectors of \mathbf{B} , $\{\mathbf{v}^j\}_{j=1}^m$, each eigenvector $\mathbf{v}^j \in \mathbb{R}^n$.

Output: m dimensional embeddings $\mathbf{y}_i = (v_i^1, \dots, v_i^m)$

We have seen three embedding algorithms so far in this section: ISOMAP, LE, LTSA, which all come with a certain performance guarantee. On the other hand, locally linear embedding (LLE, Roweis & Saul (2000)) is a heuristic method that utilizes a very similar idea: estimate local representations first and then align them globally. However, vanilla LLE does not perform well empirically and lacks theoretical guarantees (Ting et al., 2010, Ting & Jordan, 2018).

4.3 “Horseshoe” effects, neighbor embedding algorithms, and selecting independent eigenvectors

Algorithms that use eigenvectors, such as DM, are among the most promising and well-studied in ML (see Sections 5.1,5.2,5.4). Unfortunately, such algorithms fail when the data manifold has a large aspect ratio (such as a long, thin strip, or a thin torus). This problem has been called *the Repeated Eigendirection Problem (REP)* and has been demonstrated for LLE, LE, LTSA, HE (Goldberg et al., 2008), and is pervasive in real data sets.

From a differential geometric standpoint, the REP is a drop in the rank of the embedding Jacobian, due to eigenvectors (or eigenfunctions, in the limit) that are harmonics of previous ones, as shown in Figure 3. For example, for a rectangular strip (and a finite sample), the scatterplot of $(hv_i^1, hv_i^2)_{i=1,\dots,n}$ from step 3 of the DM follows a parabola; hence, it is a 1-dimensional mapping, even though the rectangle is 2-dimensional. This fact is a relevant diagnosis for REP in practice: when an embedding looks like a “horseshoe”, this may not represent a property of the data, but an artifact signalling that one of the data dimensions is collapsed, or poorly reflected in the embedding (Diaconis et al., 2008).

4.3.1 Relaxation-based neighbor embedding algorithms

The pervasiveness of the REP stimulated the development of algorithms that balance attraction between neighbors in the original space, with repulsion between neighbors in the embedding space (van der Maaten & Hinton, 2008, McInnes et al., 2018, Jacomy et al., 2014, Carreira-Perpiñan, 2010, Im et al., 2018). Usually, the embedding coordinates \mathbf{Y} are optimized iteratively until equilibrium is reached.

The T-SNE algorithm van der Maaten & Hinton (2008), one variant of which Böhm et al. (2022) we briefly describe here, exemplifies this approach.

STOCHASTIC NEIGHBOR EMBEDDING (SNE), proposed in Hinton & Roweis (2002), change neighborhood relationship from a hard 0-1 coding to conditional probabilities. The algorithm computes two sets of conditional probabilities: p_{ij} which models the probability of $\mathbf{x}_i, \mathbf{x}_j$ being neighbors (and is the algorithm input), and q_{ij} that models the probability of output points $\mathbf{y}_i, \mathbf{y}_j$ being neighbors. In van der Maaten & Hinton (2008), the authors proposed to use a Student-t distribution to model these conditional probabilities and, as T-SNE, this algorithm became widely used.

In more detail, from p_{ij} and q_{ij} , T-SNE constructs two similarity matrices; \mathbf{V} is the similarity between data points, calculated as $\mathbf{V} = (\mathbf{D}^{-1}\mathbf{K} + \mathbf{K}\mathbf{D}^{-1})/(2n)$, where \mathbf{K} denotes the k -nearest neighbor similarity matrix. The matrix $\mathbf{W} = [\mathbf{W}_{ij}]_{i,j=1}^n$ represents similarities in the embedding space; $\mathbf{W}_{ij} = \frac{1}{1 + \mathbf{A}_{ij}^{out}}$ where $\mathbf{A}_{ij}^{out} = \|\mathbf{y}_i - \mathbf{y}_j\|^2$ is the squared distance matrix in the embedding space, a dense matrix.

The T-SNE algorithm starts with arbitrary coordinates $\mathbf{Y} \in \mathbb{R}^{n \times m}$, and iteratively updates them by gradient descent to minimize the following loss function, which is akin to a cross-entropy (Hinton & Roweis, 2002, van der Maaten & Hinton, 2008).

$$\mathcal{L}^{t-SNE} = - \sum_{i,j} \frac{1}{n} \mathbf{V}_{ij} \ln \mathbf{W}_{ij} + \ln \sum_{ij} \mathbf{W}_{ij}. \quad (7)$$

In the above, $\sum_{ij} \mathbf{W}_{ij} = w_{tot}$ normalizes the entries of \mathbf{W} to 1. Thus, the original aim of T-SNE is to match the (normalized) data weights by the (normalized) embedding weights around each point, which motivates the name *Stochastic Neighbor Embedding* (SNE, Hinton & Roweis (2002)).

Uniform manifold approximation and projection (UMAP, McInnes et al. (2018)) is another popular heuristic method. On a high level, UMAP minimizes the mismatches between topological representations of high-dimensional data set $\{\mathbf{x}_i\}_{i=1}^n$ and its low-dimensional embeddings \mathbf{y}_i . Theories of UMAP are still very limited.

T-SNE has the advantage of being sensitive to local structure and to clusters in data (Linderman & Steinerberger, 2019, Kobak et al., 2020) (but does not explicitly preserve the global structure). We note that this propensity for finding clusters comes partly from the choice of neighborhood graph (Section 5.1). However, this is not the whole story. Recently, it has been shown that this property stems from the gradient of the loss function \mathcal{L}^{t-SNE} , which has the form

$$\frac{\partial \mathcal{L}^{t-SNE}}{\partial \mathbf{y}_i} = - \sum_{ij} \mathbf{V}_{ij} \mathbf{W}_{ij} (\mathbf{y}_i - \mathbf{y}_j) + \frac{n}{\rho} \sum_{ij} \frac{\mathbf{W}_{ij}}{w_{tot}} (\mathbf{y}_i - \mathbf{y}_j). \quad (8)$$

In the above, the first term is an attraction between graph neighbors, while the second represents repulsive forces between the embedded points $\mathbf{y}_{1:n}$ (Böhm et al., 2022, Zhang et al., 2022). Note the additional important parameter ρ , which controls the trade-off between attraction and repulsion (ρ corresponds to a version of the cost with $w_{tot}^{1/\rho}$ in the second term). In Böhm et al. (2022) it is shown that varying ρ from small to large values ρ decreases the cluster separation, and makes the embedding more similar to the LE embedding. Moreover, quite surprisingly, Böhm et al. (2022) shows that by varying ρ , the T-SNE can emulate a variety of other algorithms, most notably.

UMAP (McInnes et al., 2018) and FORCEATLAS (Jacomy et al., 2014).. Other works that analyze the attraction-repulsion behavior of T-SNE are Zhang & Steinerberger (2021). One yet unsolved issue with T-SNE is the choice of the number of neighbors k . Most applications use the default $k = 90$ (Poličar et al., 2019); this choice, as well as other behaviors of this class of algorithms, are discussed in Zhang et al. (2022).

Note also that since the REP can be interpreted as extreme distortion, the RIEMANNIAN-RELAXATION (Perrault-Joncas & Meila (2014) in Section 5.5) can also, be used to improve the conditioning of an embedding in an iterative manner.

Finally, in *Minimum Variance Unfolding (MVU)*, proposed in Weinberger & Saul (2006), Arias-Castro & Pelletier (2013), repulsion is implemented via a *Semidefinite Program*, hence the embedding \mathbf{Y} is obtained by solving a convex optimization. This algorithm can be seen both as a one-shot and as an attraction-repulsion algorithm; Diaconis et al. (2008) show that MVU is related to the fastest mixing Markov chain on the neighborhood graph.

4.3.2 Avoiding the REP in spectral embeddings

For algorithms like DM, and LTSA, the REP has a theoretically straightforward solution. Given a sequence of eigenfunctions $F^1, \dots, F^{m'} \dots$ on \mathcal{M} (or eigenvectors $\mathbf{v}^1, \dots, \mathbf{v}^{m'}$ in the finite sample case), with $m' > m$, sorted by their corresponding eigenvalues, one needs to select $F^{j_1} = F^1$, then (recursively) F^{j_2}, \dots, F^{j_m} so that $\text{rank}[(dF^1)_{\mathbf{p}}, \dots, (dF^{j_m})_{\mathbf{p}}] = d$ for all $\mathbf{p} \in \mathcal{M}$. This is called *Independent Eigendirection Selection (IES)*. In a finite sample, the rank condition must be replaced with the well-conditioning of dF at the data points. Dsilva et al. (2018) proposed to measure dependence by regressing $\mathbf{v}_{j_{k+1}}$ on the previously selected $\mathbf{v}_{j_1, \dots, j_k}$; in Chen & Meila (2021), a condition number derived from the embedding metric (Section 5.5) is used to evaluate entire sets of m eigenvectors. The *manifold deflation* method Ting & Jordan (2020) proposes to bypass eigenvector selection by choosing a linear combination of all eigenvectors that are optimized w.r.t. rank. Finally, the *Low Distortion Local Eigenmaps (LDLE)* Kohli et al. (2021) solves the REP by essentially covering the data manifold with contiguous patches (discrete versions of the U neighborhoods) and performing IES on each patch separately. LDLE not only

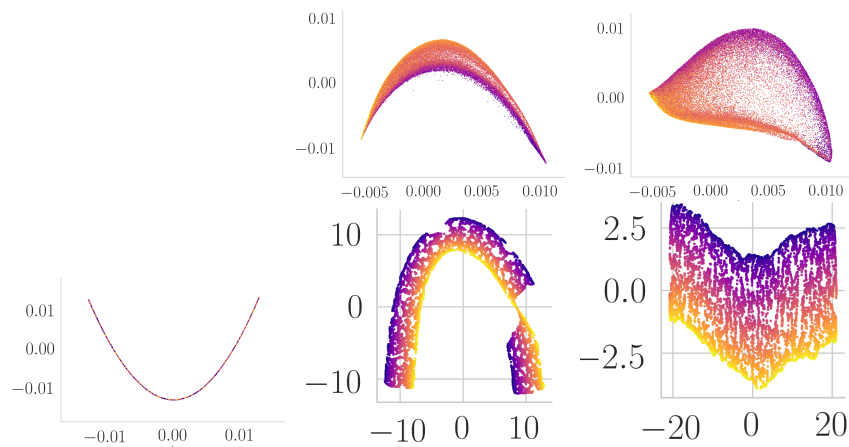


Figure 3: Embedding algorithms failing to find a full rank mapping, if they greedily select the first $m = 2$ eigenvectors, and correction by a more refined choice of eigenvectors. **Top row:** Embeddings of galaxy spectra from the SDSS (Section 6) by DM ; **middle** “horseshoe” when first 2 eigenvectors are used; **right** the same data, with selection of the second eigenvector (in this case by Chen & Meila (2021)). **Bottom row:** embeddings of a swiss roll with length 7 times the width. **Left:** first 2 eigenvectors from DM/LE; **middle** after UMAP. Note that UMAP by itself is not able to produce a full-rank embedding everywhere; the horseshoe, the two clusters, and the 1 dimensional “filament” between are all artifacts. **Right:** UMAP with selection of the second eigenvector by Chen & Meila (2021). Plots by Yu-Chia Chen.

avoids REP, but it is a first step towards the algorithmic use of charts and atlases to complement global embeddings.

In summary, attraction-repulsion algorithms such as T-SNE, which are heuristic, enjoy large popularity due in part to their immunity to the REP, while eigenvector based methods, although better grounded in theory, are less useful in practice without post-processing by an IES method. On the other hand, unlike global search in eigenvector space, a local relaxation algorithm cannot resolve the rank deficiency globally, and it may become trapped in a local optimum (Figure 3).

4.4 Summary of embedding algorithms

A variety of embedding algorithms have been developed. Here we presented representative algorithms of two types. One-shot algorithms that (typically) embed the data by eigenvectors, of which ISOMAP, DM and LTSA are the best understood as well as computationally scalable. The main drawback of this class of algorithms is the Repeated Eigendirections Problem, which requires post-processing of the eigenvectors. Neighbor embedding algorithms are (typically) iterative, starting with the output of a one-shot algorithm (LE for UMAP) or even PCA. The presence of repulsion makes these algorithms robust to REP which affects one-shot algorithms. Quantifying the repulsion, as well as the smoothness, large sample limits as well as other properties of the neighbor embedding algorithms are less developed at this time. Hence, for the moment, neighbor embedding algorithms remain heuristic for ML, while they remain useful for visualization, and clustering (for which guarantees exist Linderman & Steinerberger (2019)).

Neither type of algorithm guarantees against local singularities, such as the “crossing” in Figure 3. Currently, it is not known how these can be reliably detected or avoided. Additionally, all algorithms distort distances except in special cases (as discussed in Section 5.5).

All algorithms depend on hyperparameters: intrinsic dimension d (Section 5.3) or embedding dimension m , and k or r for the neighborhood scale (Section 5.2). Iterative algorithms often depend on additional parameters that control the repulsion (such as ρ in T-SNE), or the descent algorithm.

With respect to computation, constructing the neighborhood graph is the most expensive step typically for n large. To compound this problem, finding k or r in a principled way often requires constructing multiple graphs, one for each scale. One-shot algorithms that compute eigenvectors are quite efficient for n up to 10^6 when the matrix has a sparsity pattern that corresponds to the neighborhood graph. Neighbor embedding algorithms work, in theory, with dense matrices (e.g. \mathbf{W}); however, accelerated approximate versions for these algorithms have been developed such as the Barnes-Hut trees approximation van der Maaten (2014), and the negative sampling heuristic for UMAP Böhm et al. (2022), McInnes et al. (2018).

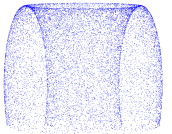


Figure 4: Data sampled from the chopped torus

5 Statistical basis of manifold learning

The output or result of manifold learning algorithms depends critically on algorithm parameters such as the type of neighborhood graph (k-nearest neighbor or radius neighbor), the neighborhood scale (k or r), and embedding dimension m (and intrinsic dimension d , in some cases).

This section is concerned with making these choices in a way that ensures some type of statistical consistency, whenever possible. Neglecting statistical consistency and stats in general is risky. In the worst case, it can lead to methods that have no limit when $n \rightarrow \infty$ (e.g. for LLE without any regularization), and in milder cases to biases (e.g. due to variations in data density), and artifacts, i.e., features of the embedding such as clusters, arms, and horseshoes that have no correspondence in the data.

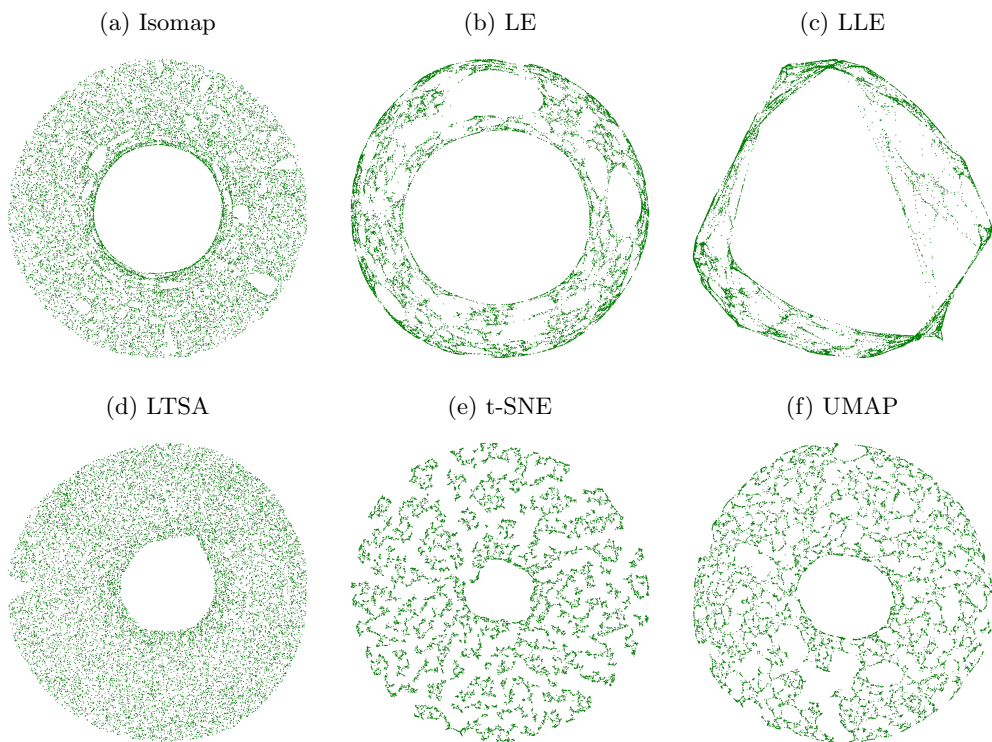


Figure 5: Embedding obtained from the algorithms in this section on a chopped torus data set with $n = 14,519$ points. This manifold cannot be embedded isometrically in $d = 2$ dimensions.

Here we discuss in more general terms what is known about graph construction methods (Section 5.1), the neighborhood scale (Section 5.2), and the intrinsic dimension (Section 5.3). We revisit the estimation of the Laplacian (a normalized version of the neighborhood graph), as the natural representation of the manifold geometry, and the basis for the DIFFUSION MAPS embedding, which can be seen as the archetypal embedding (Section 5.4). Finally, in Section 5.5, we turn to mitigate the distortions that the embedding algorithm currently induces.

5.1 Biases in ML. Effects of sampling density and graph construction

Biases due to non-uniform sampling Many embedding algorithms tend to contract regions of \mathcal{M} where the data are densely sampled and to stretch the sparsely sampled regions. In attraction-repulsion algorithms, such as t-SNE, this is explained by the repulsive forces between every pair of embedding points $\mathbf{y}_i, \mathbf{y}_j$, while the attractive forces act only along graph edges. If two dense regions are connected by fewer graph edges, repulsion will push them apart, exaggerating clusters.

The effect is similar, albeit less intuitive to explain, for one-shot algorithms, as shown in Figure 6. For DM and the graph Laplacian, the effect was calculated in Coifman & Lafon (2006); they also showed that renormalization removes the bias due to non-uniform sampling (asymptotically). Moreover, the degree values d'_i obtained in LAPLACIAN are estimators of the sampling density around data point \mathbf{x}_i . A simpler method of renormalization, applicable to low dimensional data is to use a simple estimator of the local density, and to use it to renormalize \mathbf{L}^{rw} Luo et al. (2009).

If enough samples are available, one can simply resample the data to obtain an approximately uniform distribution. For example, the *farthest point heuristic* chooses samples sequentially, with the next point being the farthest away from the already chosen points.

Effect of neighborhood graph (Figure 6) Radius neighbor graph of k -nearest neighbors? Ting et al. (2010) and later Calder & Trillos (2019) show that the k -nearest neighbor graph, with the similarity matrix with constant kernel $K(u) = 1$ exhibits qualitatively similar biases from non-uniform sampling as the simply normalized radius-neighbor graphs

5.2 Choosing the scale of neighborhood

Whatever the task, a manifold learning method requires the user to provide an external parameter, be it the number of neighbors k or the kernel bandwidth h , that sets the scale of the local neighborhood.

Theoretical results/Asymptotic results and what they mean The asymptotic results of Giné & Koltchinskii (2006), Hein et al. (2007), Ting et al. (2010) and Singer (2006) provide the necessary rates of change for h with respect to n to guarantee convergence of the respective estimate. For instance, Singer (2006) proves that the optimal bandwidth parameter for Laplacian estimation is given by $h \sim n^{-\frac{1}{d+6}}$ using a random-walk Laplacian. For the k -nearest neighbor graph, Calder & Trillos (2019) show that again for Laplacian estimation, the number of neighbors k must grow slowly with n , and a recommended rate is $k \sim n^{\frac{4}{d+4}} (\log n)^{\frac{d}{d+4}}$. The hidden constant factor in these results is not completely known, but they depend on the manifold volume, the curvature, and the *injectivity radius* τ (typically not known in practice).

With these rate-wise optimal selections of k or r , the convergence rate of estimation relating to various objects on the manifold can be established. However, all are *non-parametric* rates. More specifically, they point to the fact that the sample size n must grow *exponentially* with

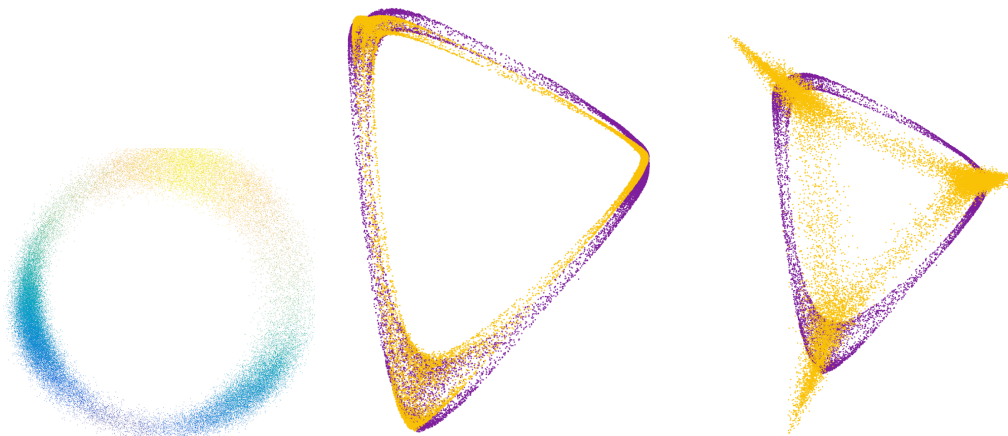


Figure 6: Effects of graph construction and renormalization, when the sampling density is highly non-uniform, exemplified on the configurations of the ethanol molecule. **Left:** original data, after preprocessing, is a noisy torus, with three regions of high density, around local minima of the potential energy. **Center:** Embeddings by DM (purple), and by the same algorithm with \mathbf{L} constructed from the k -nearest neighbor graph (yellow). The low sparse regions are stretched, while the dense regions appear like “corners” of the embedding. Note that DM *should* remove the effects of the density; in this case, the variations in density are so extreme that the effect persists. The effect is somewhat stronger for the k -nearest neighbor graph. **Right:** Embedding by DM (purple) and by LE (yellow), which uses the singly normalized \mathbf{L}^{rw} .

the dimension. For example, using the previously mentioned rate of k , together with the rate of convergence $\approx \sqrt{\frac{\log n}{k} \left(\frac{k}{n}\right)^{1/d}}$, one can calculate that, for a 10-fold decrease in error, n must increase by $\approx 10^{(d+4)/3}$. While the actual constants are not known, the statistical results suggest that, in practice, for one-shot algorithms, values of k should be sufficiently large, in order to be close to the maximum accuracy supported by the sample.

For neighbor embedding algorithms, such as t-SNE, less is known theoretically; however, practically, the defaults are for larger values of k , e.g. $k = 90$ Poličar et al. (2019) and some research suggests $k \sim n$, which would create very dense graphs.

Practical methods Unfortunately, cross-validation (CV), a widely useful model selection method in, e.g., density estimation, is not applicable in manifold learning, for the lack of a criterion to cross-validate. (However, CV is still applicable in *semi-supervised* learning on manifolds Belkin et al. (2006).) The ideas we describe below each mimic CV by choosing a criterion that measures the “self-consistency” of an embedding method at a certain scale.

For the k -nearest neighbor graph, Chen & Buja (2009) evaluates a given k with respect to the preservation of k' neighborhoods in the original graph. The method is designed to optimize for a specific embedding, so the values obtained for k depend on the embedding algorithm used. A problem to be aware of with this approach is that (see Section 5.5) most embeddings distort the data geometry, hence Euclidean neighborhoods will not be preserved, even at the optimal k .

For the radius-neighbor graph, Perraul-Joncas & Meila (2013) seeks to exploit the connection between manifold geometry, represented by the Riemannian metric, and the Laplace-Beltrami operator. The radius neighbor graph width h affects the Laplacian’s ability to recognize local isometry. Recall that local isometry is easily obtained by projecting the data on the tangent space

at some point \mathbf{x}_i . The method is specific to the estimation of the Laplace-Beltrami operator, but in this context, it can be extended to optimization over other parameters, such as kernel smoothness.

Finally, we mention a dimension estimation algorithm proposed in Chen et al. (2013), a by-product of this algorithm is a range of scales where the tangent space at a data point is well aligned with the principal subspace obtained by a local singular value decomposition. As these are scales at which the manifold looks locally linear, one can reasonably expect that they are also the correct scales at which to approximate the manifold.

5.3 Estimating the intrinsic dimension

Knowing the intrinsic dimension of data is important in itself. Additionally, some embedding algorithms (ISOMAP, LTSA), as well as all local PCA and Principal d -manifolds algorithms require the intrinsic dimension d as input.

How hard is dimension estimation? The dimension of a manifold is a non-negative integer, therefore, intuitively, it should require fewer samples to estimate than a real-valued geometric parameter. Indeed, it is known Kim et al. (2019), Genovese et al. (2012) that the *minimax rate* for dimension estimation are between n^{-2n} and $n^{-\frac{n}{D+1}}$ for a well-behaved manifold \mathcal{M} . This is an information-theoretic result, delimiting what is possible: the minimax rate is the best possible rate for any dimension estimator, on the worst possible distribution for this estimator. In the case when i.i.d. noise is added to the sample, Koltchinskii (2000) shows that the minimax rate is exponential, i.e. of order q^n for some $q < 1$. This rate is the probability that $\hat{d} \neq d$; Koltchinskii (2000) also proposes an estimator.

Unfortunately, the empirical experience belies the optimistic theoretical results. Due primarily to the presence of noise, which does not conform to the above assumptions, and secondarily to non-uniform sampling, estimating d is a hard problem, of which no satisfactorily robust solutions have been found yet (see Altan et al. (2020) for some empirical results).

Principles and methods for estimating d An idea that appears in various forms through the dimension estimation literature is to find a *local statistic* that scales with d by a known law. For example, the volume of a ball B_r of radius r contained in a manifold \mathcal{M} is proportional to r^d . If we take n samples uniformly from \mathcal{M} , the number of samples contained in B_r , denoted $\#B_r$ is proportional to nr^d , or equivalently

$$\log \#B_r = d \log r + \log n + \text{constant}. \quad (9)$$

This suggests if we fit a line to $(\log r, \log \#B_r)$, the slope of the line would represent d .

Recall that $k_{i,r}$ represents the number of radius r neighbors of data point x_i . Hence $\log k_{i,r} \approx d \log r + \text{constant}$. This is the idea of Grassberger & Procaccia (1983) who introduced the *correlation dimension* estimator given by

$$\hat{d}_C = \lim_{r \rightarrow 0} \frac{\log \frac{1}{n} \sum_{i \neq i'} \mathbf{1}_{\|x_i - x_{i'}\| \leq r}}{\log r} \quad (10)$$

In the above, $\frac{1}{n} \sum_{i \neq i'} \mathbf{1}_{\|x_i - x_{i'}\| \leq r}$, where the sum is taken over unordered pairs, is nothing else but $\frac{1}{2n} \sum_{i=1}^n (k_{i,r} - 1)$; hence, the correlation dimension uses an average number of neighbors. This estimator is easily computed for the radius neighborhood graph. To sidestep the inconvenient assumption that the sample is uniform over \mathcal{M} , other methods consider statistics such as $\frac{k_{i,2r}}{k_{i,r}} \approx 2^d$, which lead to so-called *doubling dimensions*. (Assouad, 1983)

Similarly, the covering number $\nu(r)$, representing the minimum number of boxes (in this instance) of size r needed to cover a manifold, scales like r^{-d} for r small. The *Box Counting dimension* (Falconer, 2003a) of an object is defined as

$$\hat{d}_{BC} = \lim_{r \rightarrow 0} \frac{\ln \nu(r)}{\ln \frac{1}{r}}. \quad (11)$$

If $\nu(r)$ is defined by way of balls the above becomes the well-known *Haussdorff dimension* (Falconer, 2003b). When \hat{d}_{BC} is estimated from data, the covering number represents the number of boxes (balls) to cover the data set. Note that for finite n , r cannot become too small, as in this case, every ball or box will contain a single point. The finite radius r is a scale parameter trading off bias (which increases with r), and variance (which decreases with r).

All the above estimates converge to the intrinsic dimension d when the data is sampled from a d -manifold. In practice, and with noise, their properties differ, as well as the amount of computation they need.

Modern estimators consider other statistics, such as distance to k -th nearest neighbor (Pettis et al., 1979, Costa et al., 2005), the volume of a spherical cap (Kleindessner & von Luxburg, 2015) (both statistics can be computed without knowing actual distances, just comparisons between them), or Wasserstein distance between two samples of size n on \mathcal{M} , which scales like $n^{-1/d}$ (Block et al., 2022); the algorithm of Levina & Bickel (2004), analyzed in Farahmand et al. (2007), proposes a Maximum Likelihood method based on k -nearest neighbor graphs.

An algorithm for dimension estimation in noise is proposed by Chen et al. (2013). This algorithm is based on local PCA at multiple scales; here, \hat{d}_L is the most frequent index of the maximum eigengap of the local covariance matrix. The main challenge is to establish the appropriate range of scales r at which the d principal values of the local covariances separate from the remaining eigenvalues, in noise. The algorithm can be simplified by plugging in the neighborhood radius selected to optimize the Laplacian estimator, by e.g. Joncas et al. (2017), see Section 5.2.

5.4 Estimating the Laplace-Beltrami operator

As we discussed in section 4, the Laplace-Beltrami operator $\Delta_{\mathcal{M}}$ serves as an important tool to understand the geometry of a manifold \mathcal{M} . We have seen that the eigenvectors of $\Delta_{\mathcal{M}}$ can be used to embed the data in low dimensions by the DM algorithm. Furthermore, if enough eigenvectors are computed, the embedding becomes closer to an isometry (Coifman et al., 2005).

Additionally, graph Laplacian estimators of $\Delta_{\mathcal{M}}$ are used to measure the smoothness of a function (by $\frac{1}{2}hf^T\mathbf{L}hf$), to provide regularization in supervised and semi-supervised learning on manifolds (Belkin et al., 2006, Slepčev & Thorpe, 2019), Bayesian priors (Kirichenko & van Zanten, 2017), or to define Gaussian Processes on a manifold (Borovitskiy et al., 2020).

On one hand, using graph Laplacian to estimate Laplace-Beltrami operator such as in Coifman & Lafon (2006) has been long established. Recently, more theoretical results appeared on how this estimation behaves. The **Laplace-Beltrami operator** $\Delta_{\mathcal{M}}$ acting on a twice differentiable function $f : \mathcal{M} \rightarrow \mathbb{R}$ is defined as $\Delta_{\mathcal{M}}f \equiv \text{div grad}(f)$. T

In general, two types of convergence have been studied: *pointwise* and *spectral* convergence under the formulation of Berry & Harlim (2016). Let μ be the Riemannian measure corresponding to the metric of a d dimensional manifold \mathcal{M} , $f \in C^3(\mathcal{M})$ be a real-valued function and $q(\mathbf{x})$ be the sampling density on \mathcal{M} . Further, let $\mathbf{f} = (f(\mathbf{x}_i))_{i=1}^n \in \mathbb{R}^n$. Then ideally, the two convergence paradigm of a random walk Laplacian $\mathbf{L}^{rw} = \mathbf{D}^{-1}\mathbf{L}^{un}$ defined on an h -nearest neighbor graph to its limit \mathbf{L}^∞ are given by

- Pointwise convergence: $\mathbb{E}[(\mathbf{D}^{-1}\mathbf{L}^{un}\mathbf{f})_i] \xrightarrow{n \rightarrow \infty} c\mathbf{L}^\infty f(\mathbf{x}_i) + O(h^2)$
- Spectral convergence: $\mathbb{E}[\frac{\mathbf{f}\mathbf{L}^{un}\mathbf{f}}{\mathbf{f}\mathbf{D}\mathbf{f}}] \xrightarrow{n \rightarrow \infty} c \frac{\int_{\mathbf{x} \in \mathcal{M}} f(\mathbf{x})(\mathbf{L}^\infty f)(\mathbf{x})q(\mathbf{x})d\mu(\mathbf{x})}{\int_{\mathbf{x} \in \mathcal{M}} f^2(\mathbf{x})q(\mathbf{x})d\mu(\mathbf{x})} + O(h^2)$; this type of convergence matters for spectral embedding algorithms

When the sampling density q is uniform, Belkin & Niyogi (2007) showed that pointwise convergence of random-walk Laplacian holds for $\mathbf{L}^\infty = \Delta_{\mathcal{M}}$ from an h -nearest neighbor graph. Coifman & Lafon (2006) showed that pointwise convergence holds for $\mathbf{L}^\infty = \Delta_{\mathcal{M}} - \Delta_{\mathcal{M}}q/q$ when q is not uniform. Through the renormalization, \mathbf{L} as in algorithm 3 can eliminate the bias term $\Delta q/q$ and converge to Laplace-Beltrami operator regardless of sampling density. Ting et al. (2010) further showed that for K -nearest neighbor graph, the random-walk graph Laplacian pointwisely converge to $\Delta_{\mathcal{M}}$ rescaled with $q^{2/d}$. For spectral convergence, readers are encouraged to consult Belkin & Niyogi (2007), Berry & Sauer (2019), García Trillos & Slepčev (2018), García Trillos et al. (2020).

Recently, the limits of a class of manifold learning algorithms to differential operators are studied. For a specific type called linear smoothing algorithms, these ML algorithms are proved to converge to a second-order differential operator on \mathcal{M} . For example, LE, DM converges to Laplacian operator, LTSA, HESSIAN EIGEMAPS both converge to the Frobenius norm of Hessian. Unregularized LLE, on the other hand, fails to converge to any differential operator. Details can be found in Ting & Jordan (2018).

5.5 Embedding distortions. Is isometric embedding possible?

Figure 5 shows the outputs of various embedding algorithms on a simple 2-manifold $\mathcal{M} \subset \mathbb{R}^3$. It is easily seen that the results depend on the algorithm (and parameter choices), as well as on the input (manifold and sampling density on \mathcal{M}). While all are smooth embeddings the algorithm-dependent distortions – amounting to different coordinate systems – make these outputs irreproducible and incomparable.

The presence of distortion is commonly observed empirically. Note that the distortions *do not disappear* when the sample size n increases or the sampling density is uniform, or even when the consistent graph and Laplacian are used. They are also not an effect of sampling noise. This section is concerned with recovering reproducibility, by preserving the intrinsic geometry of the data.

Attempts at isometric embedding Mathematically, the presence of distortions means that an embedding F is not isometric. Distortionless, i.e. isometric embedding is possible, as proved by a famous result of John Nash (Nash embedding theorem, Lee (2003)). Note that for a smooth embedding, the number of dimensions required is $m \geq d(d+1)/2$, the number of degrees of freedom of \mathbf{g} . The proof of Nash’s theorem is constructive, but not easily amenable to consistent, numerically stable implementation.

A more recent seminal result is that the DM embedding is isometric for large m (e.g. $m \rightarrow \infty$) (Bérard et al., 1994, Portegies, 2016). While these results are important mathematically, the fact that the embedding dimension m is required to be large makes them less interesting for data scientists/defeats the goal of dimension reduction.

Many ML methods focus on promoting isometry in local neighborhoods. Apart from the previously mentioned HESSIAN EIGENMAPS (Donoho & Grimes, 2003), LTSA (Zhang & Zha, 2004), the method of Weinberger & Saul (2006) preserve local distances in a Semidefinite Programming (SDP) framework. CONFORMAL EIGENMAP in Sha & Saul (2005) maps triangles in each neighborhood, thus succeeding in preserving angles. The works of Yu & Zhang (2010) and Lin et al.

(2013) approach global isometry by means of constructing *normal coordinates* recursively from a point $\mathbf{p} \in \mathcal{M}$, or, respectively, by mutually orthogonal *parallel vector fields*, and Verma (2011) is the first attempt to implement Nash’s construction. We note that, with the exception of Verma (2011), these methods do not guarantee an isometric embedding except in limited special cases.

Preserving isometry by estimating local distortion While finding a practical isometric embedding algorithm has been unsuccessful so far, removing the distortions is possible for any well-behaved embedding algorithm by a post-processing approach (McQueen et al., 2016). The idea is simple and general: given the (distorted) output $\mathbf{y}_1, \dots, \mathbf{y}_n$ of an embedding algorithm on data $\mathbf{x}_1, \dots, \mathbf{x}_n$, one can *estimate* the distortion incurred at each point. Once the distortions are known, whenever a distance, angle, or volume is calculated, one applies local corrections that amount to obtaining the same result as if the embedding was isometric.

This is always possible via the *push-forward metric*. Let $(\mathcal{M}, \mathbf{g})$ be a Riemannian manifold, and $F : \mathcal{M} \rightarrow \mathcal{N} = F(\mathcal{M}) \subset \mathbb{R}^m$ a smooth map, representing, e.g., the limit case of an embedding algorithm. We can endow \mathcal{N} with the *push-forward Riemannian metric* $\tilde{\mathbf{g}}$ of F at point $\mathbf{p} \in \mathcal{M}$. Let $\mathbf{u}, \mathbf{v} \in \mathcal{T}_{F(\mathbf{p})}\mathcal{N}$ be vectors in the tangent space of \mathcal{N} at point $F(\mathbf{p})$. Then the push-forward of \mathbf{g} at \mathbf{p} is defined by

$$\langle \mathbf{u}, \mathbf{v} \rangle_{\tilde{\mathbf{g}}(F_{\mathbf{p}})} \equiv \langle dF_{\mathbf{p}}^{\dagger}(\mathbf{u}), dF_{\mathbf{p}}^{\dagger}(\mathbf{v}) \rangle_{\mathbf{g}(\mathbf{p})}. \quad (12)$$

In the above, $dF_{\mathbf{p}}^{\dagger}$ is the pseudoinverse of $dF_{\mathbf{p}}$. In matrix notation (12) implies that

$$\tilde{\mathbf{g}}(F_{\mathbf{p}}) \equiv ((dF_{\mathbf{p}})^T)^{\dagger} \mathbf{g}(\mathbf{p}) (dF_{\mathbf{p}})^{\dagger} \quad (13)$$

with $dF_{\mathbf{p}}, \mathbf{g}(\mathbf{p}), \tilde{\mathbf{g}}(\mathbf{p})$ are matrices of size $d \times m$, $d \times d$ and $m \times m$ respectively, and $\mathbf{g}(\mathbf{p}), \tilde{\mathbf{g}}(\mathbf{p})$ positive semidefinite matrices of rank d . When $\mathcal{M} \subset \mathbb{R}^D$, with metric inherited from the ambient space, $\mathbf{g}(\mathbf{p}) = \mathbf{I}_d$ the unit matrix and $\tilde{\mathbf{g}}(\mathbf{p}) = ((dF_{\mathbf{p}})^T)^{\dagger} (dF_{\mathbf{p}})^{\dagger}$. Comparing (12) with (1) it is easy to see that $(F(\mathcal{M}), \tilde{\mathbf{g}})$ is isometric with the original $(\mathcal{M}, \mathbf{g})$.

Hence, if one computes for each embedding point \mathbf{y}_i the respective pushforward metric $\tilde{\mathbf{g}}_i \in \mathbb{R}^{m \times m}$, then all geometric quantities computed with the points $\mathbf{y}_1, \dots, \mathbf{y}_n$ w.r.t. $\tilde{\mathbf{g}}$ would preserve their values in the original data, subject only to sampling noise.

It remains to see how to estimate $\tilde{\mathbf{g}}$. A direct way is via (13), using an estimator of $dF(\mathbf{p})$. Another method Perrault-Joncas & Meila (2013) is via the Laplace-Beltrami operator $\Delta_{\mathcal{M}}$, namely using the Diffusion Maps Laplacian, whose properties and consistency is well studied, as seen in Section 5.4. To extract $\tilde{\mathbf{g}}$, Perrault-Joncas & Meila (2013) applies $\Delta_{\mathcal{M}}$ to a suitably chosen set of *test functions* f_{kl} , with $1 \leq k \leq l \leq m$, where $f_{kl, \mathbf{p}} = (F^k - F^k(\mathbf{p})) (F^l - F^l(\mathbf{p}))$ are pairwise products of coordinate functions, centered at point \mathbf{p} . They show that $\frac{1}{2} \Delta_{\mathcal{M}} f_{kl, \mathbf{p}}|_{(\mathbf{p})} = \tilde{\mathbf{h}}_{kl}(\mathbf{p})$, the k, l entry in the inverse pushforward metric at \mathbf{p} (algorithmically, on a sample, this operation can be easily vectorized). To obtain \mathbf{g}_i the metric at data point i , one computes the rank d pseudo-inverse (Adi Ben-Israel, 2003) of $\tilde{\mathbf{h}}_i$ by SVD. Note that $\tilde{\mathbf{h}}_i$ itself measures the local distortion at data point i . The embedding metric $\tilde{\mathbf{g}}$ and its SVD offer other insights into the embedding. For instance, the singular values of $\tilde{\mathbf{g}}$ may offer a window into estimating d by looking for a “singular value gap”. The d singular vectors form an orthonormal basis of the tangent space $\mathcal{T}_{\mathbf{p}}F(\mathcal{M})$ at point $\mathbf{p} = \mathbf{y}_i$, providing a natural framework for constructing a *normal coordinate chart* around \mathbf{p} . The non-zero singular values of $\tilde{\mathbf{h}}_i$ yield a measure of the distortion induced by the embedding around the data point \mathbf{x}_i (indeed, if the embedding were isometric to \mathcal{M} with the metric inherited from \mathbb{R}^m , then the embedding metric $\tilde{\mathbf{g}}$ would have exactly d singular values equal to 1).

This last remark can be used in many ways, such as getting a global distortion for the embedding, and hence as a tool to compare various embeddings. It can also be used to define

an objective function to minimize in order to get a more isometric embedding; such as the RIEMANNIANRELAXATION of McQueen et al. (2016).

6 Applications of manifold learning

6.1 Manifold learning in statistics

In Section 5.4 we mentioned that graph Laplacians, such as \mathbf{L} and \mathbf{L}^{norm} can generate *smoothness functionals*; given a function $f : \mathcal{M} \rightarrow \mathbb{R}$, and its values on the data points $\mathbf{f} = [f(\mathbf{x}_i)]_{i=1}^n$, the value $\frac{1}{2} \langle \mathbf{L}\mathbf{f}, \mathbf{f} \rangle$ approximates the L^2 norm $\|\nabla f\|_2^2$ on the manifold. This can be used as a regularizer in supervised or semi-supervised learning. If \mathbf{L}^{norm} is used instead of \mathbf{L} , then the smoothness is measured w.r.t. sampling distribution on \mathcal{M} .

Manifold learning by DM is closely related to *spectral clustering* (Shi & Malik, 2000, Meilă & Shi, 2001, Ng et al., 2001, von Luxburg, 2007, Meilă, 2016), as both map the data to low dimensions by the eigenvectors of a Laplacian. For clustering, it is preferable to use \mathbf{L}^{rw} the random walks Laplacian, which takes into account the data density and will exaggerate the clusters. In fact, by mapping the data to lower dimension with \mathbf{L}^{rw} , one can observe a continuum between separating clusters (if the data is clustered) and smooth embedding (for the data regions where data lie on a manifold), and even perform simultaneous embedding and clustering. In such cases, it is important to calculate a sufficient number of eigenvectors: for K clusters, there

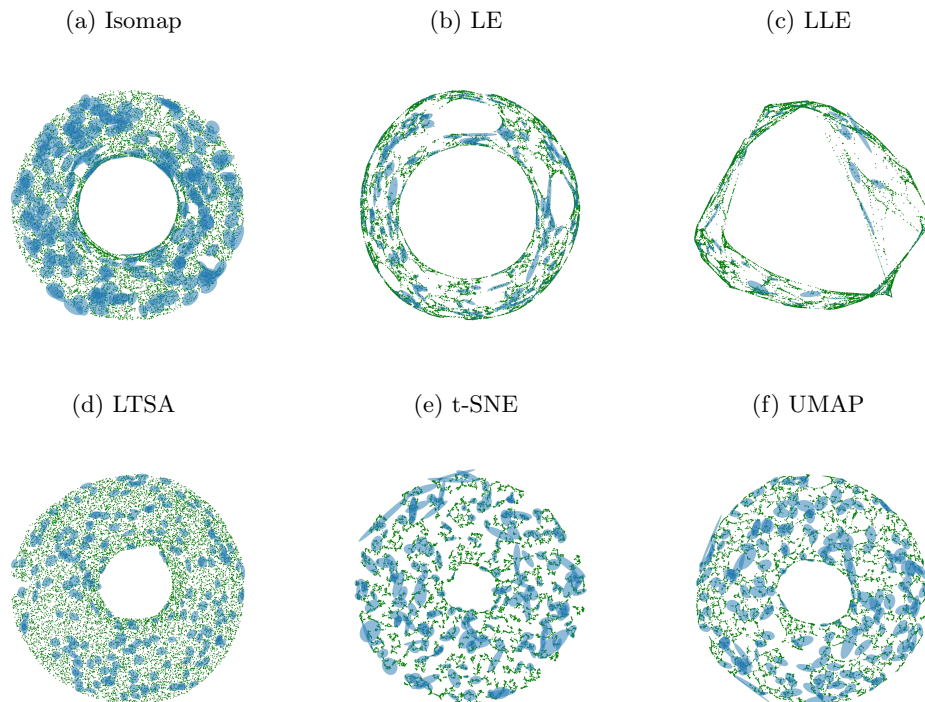


Figure 7: The embeddings from Figure 5, with the distortion $\tilde{\mathbf{h}}$ estimated at a random subset of points.

will be $K - 1$ eigenvectors indicating the clustering, and for each cluster, additional eigenvectors for a low-dimensional mapping of the data in the respective cluster. If fewer eigenvectors are used, then usually the clusters will be recovered but not the intrinsic geometry inside each cluster.

6.2 Manifold learning for visualization

Embedding algorithms are often used in the sciences for data visualization. The scientist, as well as the statistician, need to distinguish between an embedding as defined in Section 2, which preserves the geometric and topological data properties, and other mappings (occasionally also called “embeddings”) into low dimensions using embedding algorithms. The latter kind of dimension reduction is hugely popular, and its value for the sciences cannot be underestimated. However, the users of dimension reduction for visualization should be cautioned that the scientific conclusions drawn from these visualizations must be subject to careful additional scrutiny, or to a more rigorous statistical and geometric analysis. One pitfall is that when data are mapped into $m = 2$ or 3 dimensions, for visualization, without an estimation of the intrinsic dimension d , the mapping may collapse together regions of the data that are not close in the original manifold. When clusters are present because separating the clusters usually requires at least 2 dimensions, most of the clusters’ geometric structure is collapsed. Hence, once the data is separated into clusters, the cluster structure needs to be studied by additional dimension reduction. A second pitfall is the presence of artifacts – interesting geometric features caused by the embedding algorithm but not supported by the data. These can be clusters (Figure 3), , arms, holes or circles, and so on.

Before assigning scientific meaning to these features, a researcher should examine whether they are stable, by repeating the embedding with different initial points, algorithms, and algorithm parameters, as well as by perturbing or resampling the original data. To assess if the features are not large distortions, visualizing the distortion (Figure 7) can provide a valuable diagnostic. For example, when a “filament” is produced by stretching a low density region, a very common effect (see Section 5.1), the estimated distortion will show the stretching (Figure 7), while for a true filament, the distortion will be moderate .

6.3 Manifold learning in the sciences

Astronomy and astrophysics Manifold learning has been used to study data from large astronomical surveys, like the Sloan Digital Sky Survey (SDSS)². The mass distribution in the universe reveals *filaments*, i.e. one-dimensional manifolds, and dimension reduction methods, most often Principal Curves (Section 3 have been used to estimate them Chen et al. (2015)).

Spectra of galaxies are measured in thousands of frequency bands; they contain rich data about galaxies’ chemical and physical composition. By embedding these spectra in low dimensions, as in Figure 3, one can analyze the main constraints and pathways in the evolution of galaxies (Vanderplas & Connolly, 2009).

Dynamical systems Dynamical systems described by Ordinary or Partial Differential Equations are intimately related to manifolds, while they also exhibit multiscale behavior. Extensions of manifold learning can be used to understand PDE with geometric structure (Nadler et al., 2006), study the long term behavior of the system or the ensemble of its solutions Dsilva et al. (2016, 2018).

²www.sdss.org

Chemistry The accurate simulation of atomical and molecular systems plays a major role in modern chemistry. *Molecular Dynamics (MD)* simulations from carefully designed, complex quantic models can take millions of computer hours; however, simulations can still be less expensive than conducting experiments, and they return data at a level of detail not achievable in most experiments. Manifold learning is used to discover *collective coordinates*, i.e. low dimensional descriptors that approximate well the larger scale behavior of atomic, molecular, and other large particle systems (Boninsegna et al., 2015, A. et al., 2012, Noé & Clementi, 2017). In these examples, the systems can be in equilibrium, or evolving in time, and in the latter case, the collective coordinates describe the saddle points in the trajectory, or the folding mechanism of a large molecule (Rohrdanz et al., 2011, Das et al., 2006).

Manifold embedding is also used to create low dimensional maps of families of molecules and materials by the similarity of their properties (Ceriotti et al., 2013, Isayev et al., 2015).

Biological sciences In neuroscience and the biological sciences, manifold embeddings are widely used to summarize neural recordings (Connor & Rozell, 2016, Cunningham & Yu, 2014), to describe cell evolution (Herring et al., 2018)

7 Conclusion

In practice, ML is overwhelmingly used for visualization (Section 6) and with small data sets. But ML can do much more. Efficient software now exists (McQueen et al. (2016), Poličar et al. (2019), etc) which can embed truly large, high-dimensional data (for example SDSS). In these cases, ML helps practitioners understand the data, by e.g. its intrinsic dimension, or by interpreting the manifold coordinates (Koelle et al., 2022, Boninsegna et al., 2015, Vanderplas & Connolly, 2009). For real data, a manifold learning algorithm has the effect of smoothing the data and suppressing/removing variation orthogonal to the manifold, which can be regarded as noise, just like in PCA. Finally, again similarly to PCA, ML can effectively reduce the data to $m \ll D$ dimensions, while preserving features predictive for future statistical inferences. Some inferences, such as regression, can be performed on manifold data without manifold estimation, by for example, local linear regression (Aswani et al., 2011), or via Gaussian Processes (Borovitskiy et al., 2020). A GP on a manifold can be naturally defined via the Laplacian $\Delta_{\mathcal{M}}$.

Even when only visualization is desired, care must be taken to ensure the reproducibility of the results. The implicit assumption that $m = 2$ is sufficient for embedding the data should be validated. Attention to be paid when the embedding is interpreted: are the features observed really in the data or artifacts of the algorithm?

What we omitted We surveyed the state-of-the-art knowledge on the main problems and methods of manifold learning, focusing on the algorithms that are proven to recover the manifold structure through learning a smooth embedding.

Among the topics we had to leave out, manifold learning in noise is perhaps the most important one. Noise makes ML significantly more difficult, by introducing biases and slowing the convergence of estimators. This is an active area of research, but the estimation of geometric quantities like tangent space and reach in the presence of noise have been studied (Aamari & Levrard (2018, 2019), etc); the theoretical results of manifold recovery in noise were mentioned in Section 3.

The *reach*, or *injectivity radius* $\tau(\mathcal{M})$ of manifold measures how close to itself \mathcal{M} can be. In other words, $\tau(\mathcal{M})$ is the largest radius a ball can have, so that, for any $\mathbf{p} \in \mathcal{M}$, if it is tangent to the manifold in \mathbf{p} , it does not intersect \mathcal{M} in any other point. Large τ implies larger curvature

(a subspace has infinite τ) and easier estimation of \mathcal{M} (Genovese et al., 2012, Fefferman et al., 2016, Aamari & Levrard, 2018, 2019). A manifold can have borders; ML with borders is studied for example in Singer & Wu (2012), different convergence rates appear when data are sampled close to the border.

Another useful task is embedding a new data point $\mathbf{x} \in \mathbb{R}^D$ onto an existing embedding $F(\mathcal{M})$; this is often called *Nystrom* embedding (e.g. Chatalic et al. (2022)). Conversely, if $\mathbf{y} \in \mathbb{R}^m$ is a new point on the embedding $F(\mathcal{M})$, obtained e.g. by following a curve in the low dimensional representation of \mathcal{M} , how do we map it back to \mathbb{R}^D ? This is usually done by interpolation.

References

- A. TG, Ceriotti M, Parrinello M. 2012. Using sketch-map coordinates to analyze and bias molecular dynamics simulations. *Proceedings of the National Academy of Science, USA* 109:5196–201
- Aamari E, Levrard C. 2018. Stability and minimax optimality of tangential delaunay complexes for manifold reconstruction. *Discrete & Computational Geometry* 59(4):923–971
- Aamari E, Levrard C. 2019. Nonasymptotic rates for manifold, tangent space and curvature estimation. *Ann. Stat.* 47(1):177–204
- Adi Ben-Israel TNEG. 2003. Generalized inverses: Theory and applications. New York: Springer New York, NY
- Altan E, Solla SA, Miller LE, Perreault EJ. 2020. Estimating the dimensionality of the manifold underlying multi-electrode neural recordings. *bioRxiv*
- Arias-Castro E, Pelletier B. 2013. On the convergence of maximum variance unfolding. *Journal of Machine Learning Research* 14:1747–1770
- Assouad P. 1983. Plongements lipschitziens dans $\{\{r\}\}^n$. *Bulletin de la Société Mathématique de France* 111:429–448
- Aswani A, Bickel P, Tomlin C. 2011. Regression on manifolds: Estimation of the exterior derivative. *The Annals of Statistics* 39(1):48–81
- Baraniuk RG, Wakin MB. 2009. Random projections of smooth manifolds. *Foundations of Computational Mathematics* 9(1):51–77
- Belkin M, Niyogi P. 2002. Laplacian eigenmaps and spectral techniques for embedding and clustering. In *Advances in Neural Information Processing Systems 14*. Cambridge, MA: MIT Press
- Belkin M, Niyogi P. 2003. Laplacian eigenmaps for dimensionality reduction and data representation. *Neural Computation* 15(6):1373–1396
- Belkin M, Niyogi P. 2007. Convergence of laplacian eigenmaps. In *Advances in Neural Information Processing Systems 19*, eds. B Schölkopf, JC Platt, T Hoffman. MIT Press, 129–136
- Belkin M, Niyogi P, Sindhvani V. 2006. Manifold regularization: A geometric framework for learning from labeled and unlabeled examples. *Journal of Machine Learning Research* 7(85):2399–2434

- Bérard P, Besson G, Gallot S. 1994. Embedding Riemannian manifolds by their heat kernel. *Geometric Functional Analysis* 4(4):373–398
- Bernstein M, de Silva V, Langford JC, Tennenbaum J. 2000. Graph approximations to geodesics on embedded manifolds. <http://web.mit.edu/cocosci/isomap/BdSLT.pdf>
- Berry T, Harlim J. 2016. Variable bandwidth diffusion kernels. *Applied and Computational Harmonic Analysis* 40(1):68–96
- Berry T, Sauer T. 2019. Consistent manifold representation for topological data analysis
- Block A, Jia Z, Polyanskiy Y, Rakhlin A. 2022. Intrinsic dimension estimation using wasserstein distance. *Journal of Machine Learning Research* 23(313):1–37
- Boninsegna L, Gobbo G, Noé F, Clementi C. 2015. Investigating molecular kinetics by variationally optimized diffusion maps. *Journal of chemical theory and computation* 11(12):5947–5960
- Borovitskiy V, Terenin A, Mostowsky P, Deisenroth (he/him) M. 2020. Matérn gaussian processes on riemannian manifolds, In *Advances in Neural Information Processing Systems*, eds. H Larochelle, M Ranzato, R Hadsell, M Balcan, H Lin, vol. 33, pp. 12426–12437, Curran Associates, Inc.
- Böhm JN, Berens P, Kobak D. 2022. Attraction-repulsion spectrum in neighbor embeddings. *Journal of Machine Learning Research* 23(95):1–32
- Calder J, Trillos NG. 2019. Improved spectral convergence rates for graph laplacians on epsilon-graphs and k-nn graphs. *ArXiv* abs/1910.13476
- Carreira-Perpiñán MA. 2010. The elastic embedding algorithm for dimensionality reduction, ICML’10, p. 167–174, Madison, WI, USA: Omnipress
- Cerioti M, Tribello GA, Parrinello M. 2013. Demonstrating the transferability and the descriptive power of sketch-map. *Journal of Chemical Theory and Computation* 9(3):1521–1532 PMID: 26587614
- Chatalic A, Schreuder N, Rosasco L, Rudi A. 2022. Nyström kernel mean embeddings, In *Proceedings of the 39th International Conference on Machine Learning*, eds. K Chaudhuri, S Jegelka, L Song, C Szepesvari, G Niu, S Sabato, vol. 162 of *Proceedings of Machine Learning Research*, pp. 3006–3024, PMLR
- Chen G, Little AV, Maggioni M. 2013. Multi-resolution geometric analysis for data in high dimensions. Boston: Birkhäuser Boston, 259–285
- Chen L, Buja A. 2009. Local Multidimensional Scaling for nonlinear dimension reduction, graph drawing and proximity analysis. *Journal of the American Statistical Association* 104(485):209–219
- Chen YC, Genovese CR, Wasserman L. 2015. Asymptotic theory for density ridges. *The Annals of Statistics* 43(5):1896–1928
- Chen YC, Meila M. 2021. The decomposition of the higher-order homology embedding constructed from the k-laplacian, In *Advances in Neural Information Processing Systems*, eds. M Ranzato, A Beygelzimer, Y Dauphin, P Liang, JW Vaughan, vol. 34, pp. 15695–15709, Curran Associates, Inc.

- Chmiela S, Tkatchenko A, Sauceda H, Poltavsky I, Schütt KT, Müller KR. 2017. Machine learning of accurate energy-conserving molecular force fields. *Science Advances*
- Coifman RR, Lafon S. 2006. Diffusion maps. *Applied and Computational Harmonic Analysis* 30(1):5–30
- Coifman RR, Lafon S, Lee A, Maggioni, Warner, Zucker. 2005. Geometric diffusions as a tool for harmonic analysis and structure definition of data: Diffusion maps, In *Proceedings of the National Academy of Sciences*, pp. 7426–7431
- Connor M, Rozell C. 2016. Unsupervised learning of manifold models for neural coding of physical transformations in the ventral visual pathway, In *Neural Information Processing Systems (NIPS) Workshop, Brains and Bits: Neuroscience Meets Machine Learning*. Barcelona, Spain
- Costa J, Girotra A, Hero A. 2005. Estimating local intrinsic dimension with k-nearest neighbor graphs, In *IEEE/SP 13th Workshop on Statistical Signal Processing, 2005*, pp. 417–422
- Cunningham JP, Yu BM. 2014. Dimensionality reduction for large-scale neural recordings. *Nature Neuroscience* 16:1500—1509
- Das P, Moll M, Stamati H, Kaviraki L, Clementi C. 2006. Low-dimensional, free-energy landscapes of protein-folding reactions by nonlinear dimensionality reduction. *Proceedings of the National Academy of Sciences* 103(26):9885–9890
- Diaconis P, Goel S, Holmes S. 2008. Horseshoes in multidimensional scaling and local kernel methods. *The Annals of Applied Statistics* 2(3):777 – 807
- do Carmo M. 1992. Riemannian geometry. Springer
- Donoho DL, Grimes C. 2003. Hessian eigenmaps: Locally linear embedding techniques for high-dimensional data. *Proceedings of the National Academy of Sciences* 100(10):5591–5596
- Dsilva CJ, Talmon R, Coifman RR, Kevrekidis IG. 2018. Parsimonious representation of nonlinear dynamical systems through manifold learning: A chemotaxis case study. *Appl. Comput. Harmon. Anal.* 44(3):759–773
- Dsilva CJ, Talmon R, Gear CW, Coifman RR, Kevrekidis IG. 2016. Data-driven reduction for a class of multiscale fast-slow stochastic dynamical systems. *SIAM J. Appl. Dyn. Syst.* 15(3):1327–1351
- Falconer K. 2003a. Alternative definitions of dimension, chap. 3. John Wiley & Sons, Ltd, 39–58
- Falconer K. 2003b. Hausdorff measure and dimension, chap. 2. John Wiley & Sons, Ltd, 27–38
- Farahmand Am, Szepesvári C, Audibert JY. 2007. Manifold-adaptive dimension estimation, In *Proceedings of the 24th International Conference on Machine Learning, ICML '07*, p. 265–272, New York, NY, USA: Association for Computing Machinery
- Fefferman C, Mitter S, Narayanan H. 2016. Testing the manifold hypothesis. *J. Amer. Math. Soc.* 29(4):983–1049
- García Trillos N, Gerlach M, Hein M, Slepčev D. 2020. Error estimates for spectral convergence of the graph laplacian on random geometric graphs toward the laplace-beltrami operator. *Foundations of Computational Mathematics* 20(4):827–887

- García Trillos N, Slepčev D. 2018. A variational approach to the consistency of spectral clustering. *Applied and Computational Harmonic Analysis* 45(2):239–281
- Genovese CR, Perone-Pacífico M, Verdinelli I, Wasserman LA. 2012. Minimax manifold estimation. *Journal of Machine Learning Research* 13:1263–1291
- Giné E, Koltchinskii V. 2006. Concentration inequalities and asymptotic results for ratio type empirical processes. *The Annals of Probability* 34(3):1143 – 1216
- Goldberg Y, Zakai A, Kushnir D, Ritov Y. 2008. Manifold learning: The price of normalization. *Journal of Machine Learning Research* 9(63):1909–1939
- Grassberger P, Procaccia I. 1983. Measuring the strangeness of strange attractors. *Physica D: Nonlinear Phenomena* 9(1):189–208
- Hastie T, Stuetzle W. 1989. Principal curves. *Journal of the American Statistical Association* 84(406):502–516
- Hegde C, Wakin M, Baraniuk R. 2007. Random projections for manifold learning, In *Advances in Neural Information Processing Systems*, eds. J Platt, D Koller, Y Singer, S Roweis, vol. 20. Curran Associates, Inc.
- Hein M, Audibert J, von Luxburg U. 2007. Graph laplacians and their convergence on random neighborhood graphs. *Journal of Machine Learning Research* 8:1325–1368
- Herring CA, Banerjee A, McKinley ET, Simmons AJ, Ping J, et al. 2018. Unsupervised trajectory analysis of Single-Cell RNA-Seq and imaging data reveals alternative tuft cell origins in the gut. *Cell Syst* 6(1):37–51.e9
- Hinton GE, Roweis S. 2002. Stochastic neighbor embedding, In *Advances in Neural Information Processing Systems*, eds. S Becker, S Thrun, K Obermayer, vol. 15. MIT Press
- Im DJ, Verma N, Branson K. 2018. Stochastic neighbor embedding under f-divergences
- Isayev O, Fourches D, Muratov EN, Oses C, Rasch K, et al. 2015. Materials cartography: Representing and mining materials space using structural and electronic fingerprints. *Chemistry of Materials* (27):735–743
- I.T.Jolliffe. 2002. Principal component analysis. Springer Series in Statistics. Springer New York, NY
- Jacomy M, Venturini T, Heymann S, Bastian M. 2014. Forceatlas2, a continuous graph layout algorithm for handy network visualization designed for the gephi software. *PLOS ONE* 9(6):1–12
- Joncas D, Meila M, McQueen J. 2017. Improved graph laplacian via geometric Self-Consistency. In *Advances in Neural Information Processing Systems 30*, eds. I Guyon, UV Luxburg, S Bengio, H Wallach, R Fergus, S Vishwanathan, R Garnett. Curran Associates, Inc., 4457–4466
- Kim J, Rinaldo A, Wasserman LA. 2019. Minimax rates for estimating the dimension of a manifold. *J. Comput. Geom.* 10(1):42–95
- Kirichenko A, van Zanten H. 2017. Estimating a smooth function on a large graph by Bayesian Laplacian regularisation. *Electronic Journal of Statistics* 11(1):891 – 915

- Kleindessner M, von Luxburg U. 2015. Dimensionality estimation without distances, In *AISTATS*
- Kobak D, Linderman G, Steinerberger S, Kluger Y, Berens P. 2020. Heavy-tailed kernels reveal a finer cluster structure in t-sne visualisations, In *Machine Learning and Knowledge Discovery in Databases*, eds. U Brefeld, E Fromont, A Hotho, A Knobbe, M Maathuis, C Robardet, pp. 124–139, Cham: Springer International Publishing
- Koelle SJ, Zhang H, Meila M, Chen YC. 2022. Manifold coordinates with physical meaning. *Journal of Machine Learning Research* 23(133):1–57
- Kohli D, Cloninger A, Mishne G. 2021. Ldle: Low distortion local eigenmaps. *Journal of Machine Learning Research* 22(282):1–64
- Koltchinskii VI. 2000. Empirical geometry of multivariate data: a deconvolution approach. *The Annals of Statistics* 28(2):591 – 629
- Kruskal JB. 1964. Multidimensional scaling by optimizing goodness of fit to a nonmetric hypothesis. *Psychometrika* 29(1):1–27
- Lee JM. 2003. Introduction to smooth manifolds. Springer-Verlag New York
- Levina E, Bickel PJ. 2004. Maximum likelihood estimation of intrinsic dimension, In *Advances in Neural Information Processing Systems 17 NIPS 2004, December 13-18, 2004, Vancouver, British Columbia, Canada*, pp. 777–784
- Lin B, He X, Zhang C, Ji M. 2013. Parallel vector field embedding. *Journal of Machine Learning Research* 14(90):2945–2977
- Linderman GC, Steinerberger S. 2019. Clustering with t-sne, provably. *SIAM Journal on Mathematics of Data Science* 1(2):313–332
- Luo C, Safa I, Wang Y. 2009. Approximating gradients for meshes and point clouds via diffusion metric. *Computer Graphics Forum* 28(5):1497–1508
- McInnes L, Healy J, Melville J. 2018. Umap: Uniform manifold approximation and projection for dimension reduction. *arXiv preprint arXiv:1802.03426*
- McQueen J, Meila M, Joncas D. 2016. Nearly isometric embedding by relaxation, In *Advances in Neural Information Processing Systems*, eds. D Lee, M Sugiyama, U Luxburg, I Guyon, R Garnett, vol. 29. Curran Associates, Inc.
- McQueen J, Meila M, VanderPlas J, Zhang Z. 2016. Megaman: Scalable manifold learning in python. *Journal of Machine Learning Research* 17
- Meilă M, Shi J. 2001. A random walks view of spectral segmentation, In *Proceedings of the Eighth International Workshop on Artificial Intelligence and Statistics*, eds. TS Richardson, TS Jaakkola, vol. R3 of *Proceedings of Machine Learning Research*, pp. 203–208, PMLR. Reissued by PMLR on 31 March 2021.
- Meilă M. 2016. Spectral clustering : a tutorial for the 2010 ' s
- Mohammed K, Narayanan H. 2017. Manifold learning using kernel density estimation and local principal components analysis. *arxiv* 1709.03615

- Nadler B, Lafon S, Coifman R, Kevrekidis I. 2006. Diffusion maps, spectral clustering and eigenfunctions of Fokker-Planck operators, In *Advances in Neural Information Processing Systems 18*, eds. Y Weiss, B Schölkopf, J Platt, pp. 955–962, Cambridge, MA: MIT Press
- Ng A, Jordan M, Weiss Y. 2001. On spectral clustering: Analysis and an algorithm, In *Advances in Neural Information Processing Systems*, eds. T Dietterich, S Becker, Z Ghahramani, vol. 14. MIT Press
- Noé F, Clementi C. 2017. Collective variables for the study of long-time kinetics from molecular trajectories: theory and methods. *Current Opinion in Structural Biology* 43:141–147
- Ozertem U, Erdogmus D. 2011. Locally defined principal curves and surfaces. *Journal of Machine Learning Research* 12(34):1249–1286
- Perrault-Joncas D, Meila M. 2013. Non-linear dimensionality reduction: Riemannian metric estimation and the problem of geometric discovery. *ArXiv e-prints*
- Perrault-Joncas D, Meila M. 2014. Improved graph laplacian via geometric self-consistency. *ArXiv e-prints*
- Pettis KW, Bailey TA, Jain AK, Dubes RC. 1979. An intrinsic dimensionality estimator from near-neighbor information. *IEEE Transactions on Pattern Analysis and Machine Intelligence* PAMI-1(1):25–37
- Poličar PG, Stražar M, Zupan B. 2019. opentsne: a modular python library for t-sne dimensionality reduction and embedding. *bioRxiv*
- Portegies JW. 2016. Embeddings of Riemannian manifolds with heat kernels and eigenfunctions. *Communications on Pure and Applied Mathematics* 69(3):478–518
- Ram P, Lee D, March W, Gray A. 2009. Linear-time algorithms for pairwise statistical problems, In *Advances in Neural Information Processing Systems*, eds. Y Bengio, D Schuurmans, J Lafferty, C Williams, A Culotta, vol. 22. Curran Associates, Inc.
- Rohrdanz MA, Zheng W, Maggioni M, Clementi C. 2011. Determination of reaction coordinates via locally scaled diffusion map. *The Journal of chemical physics* 134(12)
- Rosenberg S. 1997. The laplacian on a riemannian manifold: An introduction to analysis on manifolds. London Mathematical Society Student Texts. Cambridge University Press
- Roweis S, Saul L. 2000. Nonlinear dimensionality reduction by locally linear embedding. *Science* 290(5500):2323–2326
- Sha F, Saul LK. 2005. Analysis and extension of spectral methods for nonlinear dimensionality reduction, ICML '05. New York, NY, USA: Association for Computing Machinery
- Shi J, Malik J. 2000. Normalized cuts and image segmentation. *IEEE Transactions on Pattern Analysis and Machine Intelligence* 22(8):888–905
- Singer A. 2006. From graph to manifold laplacian: The convergence rate. *Applied and Computational Harmonic Analysis* 21(1):128–134 Special Issue: Diffusion Maps and Wavelets
- Singer A, Wu HT. 2012. Vector diffusion maps and the connection laplacian. *Communications on Pure and Applied Mathematics* 65(8):1067–1144

- Slepčev D, Thorpe M. 2019. Analysis of ℓ_1 -laplacian regularization in semisupervised learning. *SIAM Journal on Mathematical Analysis* 51(3):2085–2120
- Tenenbaum JB, de Silva V, Langford JC. 2000. A global geometric framework for nonlinear dimensionality reduction. *Science* 290(5500):2319–2323
- Ting D, Huang L, Jordan MI. 2010. An analysis of the convergence of graph laplacians, In *Proceedings of the 27th International Conference on Machine Learning (ICML-10)*, pp. 1079–1086
- Ting D, Jordan MI. 2018. On nonlinear dimensionality reduction, linear smoothing and autoencoding. *arXiv: Machine Learning*
- Ting D, Jordan MI. 2020. Manifold learning via manifold deflation
- van der Maaten L. 2014. Accelerating t-sne using tree-based algorithms. *Journal of Machine Learning Research* 15(93):3221–3245
- van der Maaten L, Hinton G. 2008. Visualizing data using t-sne. *Journal of Machine Learning Research* 9:2579–2605
- Vanderplas J, Connolly A. 2009. Reducing the dimensionality of data: Locally linear embedding of sloan galaxy spectra. *The Astronomical Journal* 138(5):1365
- Verma N. 2011. Towards an algorithmic realization of nash ’ s embedding theorem
- von Luxburg U. 2007. A tutorial on spectral clustering. *Statistics and Computing* 17(4):395–416
- Weinberger KQ, Saul LK. 2006. An introduction to nonlinear dimensionality reduction by maximum variance unfolding, In *Proceedings, The Twenty-First National Conference on Artificial Intelligence and the Eighteenth Innovative Applications of Artificial Intelligence Conference, July 16-20, 2006, Boston, Massachusetts, USA*, pp. 1683–1686, AAAI Press
- Yu K, Zhang T. 2010. Improved local coordinate coding using local tangents, In *Proceedings of the 27th International Conference on International Conference on Machine Learning, ICML’10*, p. 1215–1222, Madison, WI, USA: Omnipress
- Zha H, Zhang Z. 2007. Continuum isomap for manifold learnings. *Computational Statistics & Data Analysis* 52(1):184–200
- Zhang Y, Gilbert AC, Steinerberger S. 2022. May the force be with you, In *58th Annual Allerton Conference on Communication, Control, and Computing, Allerton 2022, Monticello, IL, USA, September 27-30, 2022*, pp. 1–8, IEEE
- Zhang Y, Steinerberger S. 2021. t-sne, forceful colorings and mean field limits. *CoRR* abs/2102.13009
- Zhang Z, Zha H. 2004. Principal manifolds and nonlinear dimensionality reduction via tangent space alignment. *SIAM J. Scientific Computing* 26(1):313–338